The transcription factor Pdr802 regulates *Cryptococcus neoformans* Titan cell production and pathogenicity

Julia C. V. Reuwsaat[1,2], Heryk Motta[1], Daniel P. Agustinho[2], Holly Brown[2], Andrew L. Chang[2], Livia Kmetzsch[1,3,4], and Tamara L. Doering[2,4].

[1]Molecular Biology of Pathogens Laboratory, Biotechnology Center, Universidade Federal do Rio Grande do Sul, Porto Alegre, Brazil.

[2]Department of Molecular Microbiology, Washington University School of Medicine, Washington University, St. Louis, Missouri, USA.

[3]Department of Molecular Biology and Biotechnology, Universidade Federal do Rio Grande do Sul, Porto Alegre, Brazil.

[4] Corresponding authors: liviak@cbiot.ufrgs.br, doering@wustl.edu

Running head: Role of Pdr802 in *Cryptococcus neoformans* virulence.

ABSTRACT

Cryptococcus neoformans is a ubiquitous, opportunistic fungal pathogen that kills almost 200,000 people worldwide each year. It is acquired when mammalian hosts inhale the infectious propagules; these are deposited in the lung and, in the context of immunocompromise, may disseminate to the brain to cause lethal meningoencephalitis. Once inside the host, *C. neoformans* cells develop a variety of features that help them avoid immune recognition, including display of a polysaccharide capsule that impairs phagocytosis and the production of giant (Titan) cells. The transcription factor Pdr802 is one regulator of these responses to the host environment. Expression of the corresponding gene is highly induced under host-like conditions *in vitro* and is critical for *C. neoformans* dissemination and virulence in a mouse model of infection. Direct targets of Pdr802 include the calcineurin targets Had1 and Pmc1, which are important for *C. neoformans* virulence; the transcription factor Bzp4, which regulates cryptococcal melanization and capsule thickness; and 35 transmembrane transporters. Notably, a strain engineered to lack Pdr802 showed a dramatic increase in Titan cells, which are not phagocytosed and have diminished ability to directly cross biological barriers. This explains the reduced dissemination of *pdr802* mutant cells to the central nervous system and the consequently reduced virulence of this strain. The role of Pdr802 as a negative regulator of titanisation is thus critical for cryptococcal pathogenicity.

IMPORTANCE

The pathogenic yeast *Cryptococcus neoformans* presents a worldwide threat to human health, especially in the context of immunocompromise, and current antifungal therapy is hindered by cost, limited availability, and inadequate efficacy. After the infectious particle is inhaled, *C. neoformans* initiates a complex transcriptional program that integrates cellular responses and enables adaptation to the host lung environment. Here we describe the role of the transcription factor Pdr802 in the response to host conditions and its impact on *C. neoformans* virulence. We identified direct targets of Pdr802 and also discovered that it regulates cellular features that influence movement of this pathogen from the lung to the brain, where it causes fatal disease. These findings significantly advance our understanding of a serious disease.

INTRODUCTION

Cryptococcosis is a fungal infection caused by *Cryptococcus neoformans* and *Cryptococcus gattii. C. neoformans* is a ubiquitous opportunistic pathogen that infects mainly immunocompromised patients, while *C. gattii* is capable of infecting immunocompetent individuals (1). Cryptococcosis causes 180,000 deaths worldwide each year, including roughly 15% of all AIDS-related deaths (2), and is initiated by the inhalation of spores or desiccated yeast cells. In immunocompetent individuals, this typically causes an asymptomatic pulmonary infection that is controlled by the host immune response, although a population of *C. neoformans* may remain latent for extended periods of time (3, 4).

Under conditions of immunocompromise, cryptococci disseminate from the lung to the brain. Mechanisms that have been suggested to mediate fungal crossing of the blood-brain barrier (BBB) include transcellular migration, in which the yeast cells enter and exit vascular endothelial cells (5–8); paracellular movement, in which they cross the BBB at junctions between endothelial cells (9–11); and 'Trojan horse' crossing, whereby macrophages harboring *C. neoformans* enter the brain (12). Cryptococcal meningoencephalitis is difficult to treat and frequently lethal, for reasons that include lack of drug availability and high cost (13, 14).

The ability of *C. neoformans* to survive and proliferate in the lung, and subsequently disseminate to the brain, depends on the expression of multiple virulence traits, such as secreted factors (15, 16), a polysaccharide capsule that surrounds the cell wall (17), and the production of giant (Titan) cells (18, 19). For example, the secreted pigment melanin associates with the cell wall, where its antioxidant properties protect fungal cells from reactive oxygen species produced as a host immune defense (20–23). Urease, a metalloenzyme that converts urea to ammonia and CO_2, is secreted extracellularly and may affect the course of infection by modulating environmental pH and damaging host tissue structure (10, 11, 24).

The capsule, composed primarily of large polysaccharides (25–27), is a key cryptococcal virulence factor that impairs phagocytosis by immune cells (28–33). This dynamic entity changes its size and structure during interactions with the host or external environment (34–38), contributing to fungal adaptation (39). Capsule polysaccharides that are shed from the cell enable diagnosis of cryptococcal infection and also impede host responses (33, 40).

Titan cells are a cryptococcal morphotype that has been variously characterized as having cell wall diameter greater than 10 or 15 µm or capsule diameter that exceeds 30 µm (19, 41, 42). These cells can be polyploid and produce normal-size cells during infection (18, 43, 44). Titan cell formation is triggered by exposure to the host environment, including nutrient starvation, reduced pH, and hypoxia (45–47), although the extent of titanisation depends on the host immune response and the duration of infection (43, 48). Titan cell production appears to benefit the development of *C. neoformans* infection in the lungs, since there is reduced internalization of these large cells by host phagocytes and they are more resistant to oxidative stress than normal-size cells (18, 44). Some of these effects may be explained by the highly cross-linked capsule and thickened cell wall of Titan cells (49). In contrast, Titan cells show impaired dissemination to the brain (18, 44).

C. neoformans experiences a dramatic change in conditions upon entering a host, including altered nutrient levels and pH. To adapt to the new environment, cryptococci activate a network of transcription factors (TFs) (37, 50). For example, imbalances in ion homeostasis trigger responses from the TFs Zap1 (51), Cuf1 (52), Pho4 (53), Cir1 (54), and Crz1 (55). Alkaline pH stimulates expression of the TF Rim101, which enables growth under basic conditions and other stresses such as high salt and iron limitation; it also promotes the association of capsule polysaccharide with the cell and the formation of Titan cells (45, 56).

Overlapping TF circuits regulate cryptococcal virulence determinants, including polysaccharide capsule production and melanin synthesis. For example, Usv101, an important regulator of capsule thickness and polysaccharide shedding, also regulates

three other TFs (Gat201, Crz1, and Rim101) and multiple polysaccharide-related enzymes (57). Gat201 further regulates additional virulence-related transcription factors and the anti-phagocytic protein Blp1 (58), while Crz1 plays a central role in the maintenance of plasma membrane and cell wall stability (55, 59, 60). Crz1 expression is also modulated by the calcineurin signalling pathway, which is required for normal yeast growth at 37°C, virulence, and sexual reproduction (61). A group of TFs, including Usv101, Bzp4, Hob1, and Mbs1 (57, 62), act together to regulate melanin production; deletion of Bzp4 also alters capsule production (50).

In this study, we investigated the TF Pdr802. The corresponding gene is highly variable, based on its rate of non-synonymous mutations, which suggests it is evolving rapidly (63). Pdr802 has been implicated in *C. neoformans* virulence (37, 50, 64), but its specific role and targets are not known. We discovered that Pdr802 is induced in host-like conditions, is a negative regulator of Titan cell formation, and influences capsule thickness and phagocytosis by macrophages. These functions, as well as its regulation of *HAD1*, *PMC1* and *BZP4*, whose products act in cell wall remodeling and virulence factor production, make Pdr802 critical for both lung survival and dissemination to the brain.

RESULTS

The role of Pdr802 in *C. neoformans* virulence

The importance of Pdr802 in *C. neoformans* virulence has been demonstrated in multiple experimental models. Liu and collaborators first reported in 2008 that partial deletion of *PDR802* reduced *C. neoformans* infectivity in a competition assay of pooled *C. neoformans* strains (64). In 2015, Maier *et al* showed that a *pdr802* deletion mutant

had reduced virulence when tested individually in a short-term mouse model of infection (37). Later that year, Jung and colleagues reported that Pdr802 was necessary for full virulence in both wax moth larvae and short-term mouse infection using pooled strains (50). Most recently, Lee and collaborators showed that Pdr802 was required for brain infection (65).

To further investigate the role of Pdr802 in pathogenesis, we complemented a complete deletion strain in the KN99α background that we had previously generated (*pdr802*) (37) with the intact gene at its native locus (*PDR802*). To examine targets of Pdr802, we also constructed a strain that expresses the protein fused to mCherry at its N-terminus (Figure S1A). All of these strains lacked or expressed RNA encoding *PDR802* or its modified forms as expected (Figure S1B) and, importantly, *PDR802* was expressed at wild-type levels in the complemented and modified strains (Figure S1C).

We next assessed the long-term survival of C57BL/6 mice infected with the parental wild-type strain (KN99α), the deletion mutant (*pdr802*), or the complemented mutant (*PDR802*). In this model, mice infected with the parent or complemented strains survived for roughly three weeks, while those infected with the deletion mutant showed a striking increase in survival: all animals survived for at least 65 days and over half survived to the end of the study (100 days; Figure 1A). The lung burden measured at the time of death for *pdr802*-infected mice in this study was approximately 100-fold lower than that of wild type infections (Figure S2A), demonstrating the importance of this TF in *C. neoformans* virulence. Mean brain burden at the time of death was more similar between mutant and wild type infections (Figure S2A), although we did note some heterogeneity in this measure for *pdr802*-infected mice; animals sacrificed at around two

months of infection showed brain burden similar to WT levels (red symbols), while brain burden of mice sacrificed at day 100 ranged between zero fungal cells and WT level (blue symbols).

We next examined the time course of fungal proliferation in the lungs. As expected, the burdens of WT and the complemented mutant strains increased steadily over an 18-day interval (Figure 1B), eventually reaching roughly five logs over the inoculum. Towards the end of this time period, these cells were also detected in the blood and brain (Figure S2B). In contrast, the lung burden of *pdr802* remained close to the original inoculum throughout this period, with no mutant cells detected in the blood or brain. At a late time point of *pdr802* infection (75 days), we again noted some heterogeneity of fungal burden: one mouse had high lung burden with no dissemination, another had high lung burden with moderate brain burden, and the third had extremely low lung burden with no dissemination (Figure S2C). No colony-forming units (CFU) were detected in the blood of *pdr802*-infected mice at any point during infection. Together, these results suggest that even though the *pdr802* strain is generally hypovirulent and remains at low levels in the lung, it can occasionally reach the brain and, given enough time, accumulate there (see Discussion).

Given the dramatic effects of Pdr802 on fungal virulence, we wondered about the specific biological processes in which this transcription factor is involved. We first examined the behavior of the *pdr802* strain *in vitro*, focusing on stress conditions that might be encountered in the host. We saw no differences in growth of the *pdr802* mutant compared to WT cells under conditions that challenge cell or cell wall integrity, including sorbitol, high salt, cell wall dyes, caffeine, sodium dodecyl sulfate (SDS), or ethanol

(Figure S3A-C). The mutant also showed no altered susceptibility to elements of the host response, such as nitrosative or oxidative stresses, or in melanin production, which is implicated in cryptococcal survival and pathogenic potential (15, 20, 21). All of these results held whether growth was at 30°C, 37°C, or 37°C in the presence of 5% CO_2, which was recently described as an independent stress for *C. neoformans* (66) (Figure S3A-C). Finally, the mutant showed no difference from wild-type cells in secretion of urease (Figure S3D), which has also been implicated in *C. neoformans* virulence and brain dissemination (10, 16, 24).

Pdr802 is regulated by "host-like" conditions

We next tested the growth of the *pdr802* mutant under conditions more like those encountered inside the mammalian host, using tissue culture medium (DMEM) at 37°C in the presence of 5% CO_2. We found that although the *pdr802* mutant grew like WT in rich medium (YPD), it grew poorly in DMEM (Figure S3E-F). To test whether the mutant cells were dead or just static after growth in DMEM, we plated aliquots on solid medium to measure CFU over time (Figure 2A). The *pdr802* culture showed a dramatic decrease in viability compared to WT and the complemented strain, which was greatest in the first 24 h. This is the same time frame in which expression of the *PDR802* gene shows a striking increase, as measured by RNA-Seq (Figure 2B).

Another important feature that is induced by growth in DMEM at 37°C and 5% CO_2 is the polysaccharide capsule, which we previously reported to be regulated by Pdr802, based on negative staining with India ink (37). Fluorescence microscopy confirmed increased capsule thickness of the mutant, which reverted to WT in the complemented strain (Figure 3A). To quantify this change, we took advantage of a semi-automated

assay that we have developed (Figure S4), which measures capsules on a population scale (Figure 3B) and is therefore very sensitive. This analysis showed that the capsule thickness of *pdr802* cells resembles that of the well-studied hypercapsular mutant *pkr1* (37, 67, 68) and is completely restored to WT by complementation at the native locus (Figure 3C). Previous studies suggest that capsule thickness upon induction reflects the size of the dominant capsule polymer (glucuronoxylomannan; GXM) (69–71), which can be analyzed by agarose gel migration and blotting with anti-capsule antibodies (69). Consistent with the difference we observed in capsule thickness by imaging, this method showed decreased mobility of GXM from *pdr802* as capsule induction progressed (Figure S3G).

To validate the observations that we had made in standard 'host-like' conditions based on synthetic tissue culture medium, we conducted similar studies in mouse serum at 37°C and 5% CO_2. These conditions induced an even more pronounced hypercapsular phenotype of the *pdr802* mutant (Figures 4A and 4B), as well as reduced cell viability (Figure 4C) and increased cell wall diameter (Figure 4D).

We were intrigued by the enlarged cell body and capsule of the *pdr802* mutant cells in host-like conditions *in vitro* and decided to examine these phenotypes *in vivo*. For these studies, we isolated fungal cells from the lungs of mice at various times of infection and assessed their morphology by negative staining (Figure 5A). At each time point, the mutant cell wall diameters were larger than the controls, but while cell wall diameter size was stable for WT and complemented strains throughout the infection period, cell wall diameter of the deletion mutant trended larger at the end of the infection period (Figure 5B). In contrast, mutant capsule thickness, although initially larger than that of control

cells, remained stable through the period (~15 µm), while capsule thickness of control cells increased to that level or beyond (Figure 5C). Over time, therefore, the ratio of capsule thickness to cell wall diameter for WT and *PDR802* cells steadily increased, while it remained roughly constant for the mutant (Figure S5A). Furthermore, although the capsule diameter of *pdr802* cells consistently exceeded that of WT and complemented cells, their sizes became more comparable late in infection (Figure S5B).

Pdr802 negatively regulates Titan cells formation

We were particularly interested in the cell size phenotype of *pdr802* because Titan cells have been strongly implicated in cryptococcal pathogenesis (18). By any definition of this morphotype (cell walls greater than 10 or 15 µm in diameter or capsules greater than 30 µm in diameter), our mutant cell populations were strikingly enriched in Titan cells. For example, the fraction of mutant cells that met the capsule diameter criterion for Titan cells (30% to 60%) greatly exceeded that of control cells (0% to 30%) (Figure S5C).

To specifically test Titan cell formation by the *pdr802* strain, we subjected mutant cells to *in vitro* conditions that induce this process (47) and analyzed the resulting population by flow cytometry. Consistent with our *in vivo* observations, Titan cells constituted a much larger fraction of the population in the mutant culture (13.2%) than in the WT culture (1.62%) (Figure 6).

Titan cells are poorly engulfed by host phagocytes (18, 43), which may reflect their increased size as well as alterations in capsule and cell wall (49). We observed this reduced uptake for all strains after growth in conditions that favor titanisation (Figure 7, Titan vs YPD). Also, all strains showed a reduction in phagocytosis after capsule

induction in DMEM (Figure 7, DMEM vs YPD), which is not surprising because the capsule is antiphagocytic (29). Notably, the reduction in uptake was greatest for the *pdr802* mutant in both of these conditions, even though it showed normal engulfment when all strains were grown in the control condition (YPD). This is likely because the mutant culture is both hypercapsular and enriched in Titan cells.

Pdr802 regulates transmembrane transporters and transcription factors

To identify potential direct targets of Pdr802, we next performed ChIP-Seq analysis. We compared DNA sequences immunoprecipitated by anti-mCherry mAb from cells expressing mCherry-Pdr802, which grow similarly to WT (Figure S6), and untagged cells. Both strains were grown for 24 hours in DMEM at 37°C and 5% CO_2, as this condition induces *PDR802* expression roughly 45-fold compared to control growth in YPD (Figure 2).

Using 2-fold-enrichment over control as a cutoff value, we identified 656 peaks in mCherry-Pdr802 genomic DNA. Of these, 540 occurred within 1,000 bp upstream of transcription start sites (Data Set S1, Sheet 1), which we used as an approximation of regulatory regions. Gene Ontology (GO) enrichment analysis of the corresponding 540 genes suggested a broad regulatory role for Pdr802, as the largest target group (35 transmembrane transporters) comprised just under 9% of the total targets (Data Set S1, Sheets 7 and 8). We next applied Discriminative Regular Expression Motif Elicitation (DREME) (72) to the complete set of upstream regions to identify potential Pdr802 binding motifs (Figure S7A), which were notable for repeated TC (GA) doublets. Finally, we used qRT-PCR to measure the expression of three putative target genes, including

BZP4, in WT and *pdr802* cells after growth in DMEM. We observed expression changes consistent with Pdr802 regulation (Figure S7B, see Discussion).

A transcriptional profiling study of *C. neoformans* cells exposed to Titan cell inducing conditions *in vitro* was recently published (46). Because we had observed that the absence of *PDR802* was associated with an increase in Titan cell formation, we compared these results to our ChIP-Seq data. Of the 562 genes reported to decrease expression during Titan cell formation *in vitro*, 44 (8%) were identified in our ChIP-Seq study; 40 of these contained a Pdr802 binding motif within 1,000 bp of the start site (Data Set S2, Sheet 1). The largest functional group of these 40 genes encodes proteins related to regulation of gene expression (Data Set S2, Sheets 1- 2). Several of these putative Pdr802 targets encode transcription factors, including *STB4*, *ECM2201*, *and FZC34*. Stb4 was recently shown to be important for cryptococcal infection of the brain (65), Fzc34 is important for proper cryptococcal capsule formation (50), and Ecm2201 is essential for capsule formation and implicated in *C. neoformans* metal ion transport and chitin synthesis (37). The next largest group consists of genes encoding transmembrane transporters (Data Set S2, Sheets 1-2). Interestingly, three of these transporters (encoded by *PTP1, CNAG_07869*, and *CNAG_00598*) are upregulated during macrophage ingestion, as is *PDR802* (73).

A somewhat higher fraction of the genes reported to increase expression during Titan cell formation was identified in our ChIP-Seq study (44 of 421; 10.5%), with 37 of them exhibiting a Pdr802 binding within 1,000 bp of the start site (Data Set S2, Sheet 3). The largest group of these 37 genes encodes proteins related to general cellular metabolic processes (Data Set S2, Sheets 2-3). Among these are two genes that encode

enzymes implicated in glucan synthesis and degradation (*CNAG_00393* and *CNAG_05138*), consistent with the importance of cell wall remodeling and capsule synthesis in Titan cell production (49). Another potential target encodes the transcription factor Zfc3, which is important for *C. neoformans* capsule formation (50) and brain infectivity (65) (Data Set S2, Sheet 3).

We also examined transporters and TFs implicated as Pdr802 targets that are not related to Titan cell formation. Interestingly, Prd802 co-immunoprecipitated with promoter regions of genes encoding the glucose transporters Hxt1 and Hxs1, as well as the inositol transporters Itr2 and Itr3 (Figure 8A). Both of these hexoses serve as carbon sources for *C. neoformans* and the activity of these transporters promotes cryptococci virulence and brain infectivity (74–77). During *C. neoformans* engulfment by macrophages, *PDR802* is upregulated, together with *HXS1* and *ITR2*, while *HXT1* is downregulated (73). During *C. neoformans* infection in mice, *PDR802* and *ITR3c* are upregulated, in both lung and brain (65).

Among TFs, Pdr802 binds upstream sequences of the genes that encode Mln1 and Fzc14 (Figure 8B). Null mutants lacking either of these TFs are hypercapsular and show increased sensitivity to the antifungal drug fluconazole (50). Pdr802 also interacts with the promotor of the gene encoding Bzp4 (Figure 8B), which, as mentioned above, regulates two virulence factors (capsule (50) and melanin (50, 62)) and is required for cryptococcal pathogenicity (50). We found that *BZP4* expression was repressed by Pdr802 under host-like conditions (Figure S7B).

The most highly-enriched peak in our Pdr802 studies was in the regulatory sequence of the gene encoding Fatty acyl-CoA synthetase and RNA processing-

associated Kinase 1-like 02 (Frk102; Figure 8C), whose product is involved in cadmium sulphate tolerance and coping with endoplasmic reticulum stress, but is not important for *C. neoformans* virulence (78).

Pdr802 regulates two calcineurin target genes

The calcineurin signaling pathway is activated by calcium and governs stress response and virulence in *C. neoformans* (79–81). A significant portion of calcineurin signaling is mediated by the transcription factor Crz1 (55) mentioned above, which is highly responsive to temperature (55, 60) and important for cryptococcal virulence (55). Other calcineurin targets, however, are regulated independently of Crz1 (55, 61). This group includes the phosphatase Had1 (55, 61), which was previously shown to be important for *C. neoformans* virulence (82). The *HAD1* gene contains three Pdr802 binding motifs within 1,000 bp of its start site (Data Set S2, Sheet 4) and was also identified in our ChIP study (Figure 9A). *HAD1* expression increases upon deletion of *PDR802* (Figure 9B), further supporting that it is a Pdr802 target.

Another target of calcineurin is the vacuolar calcium transporter Pmc1 (55, 61), which is required for *C. neoformans* virulence and dissemination to the brain (83, 84). *PMC1* was identified in our ChIP-Seq analysis (Figure 9C) and has two Pdr802 binding motifs in its promoter (Data Set S2, Sheet 4). We found that Pdr802 deletion results in increased levels of *PMC1* expression after 3 hours of growth in host-like conditions (Figure 9D), although this effect dissipates by 24 hours. Because Pmc1 is important for maintenance of normal cryptococcal Ca^{2+} concentrations (83), we wondered whether this initial increase would imbalance intracellular calcium levels. We found that cytosolic calcium levels in the *pdr802* mutant are higher than those observed in WT and

complemented strains after 24 hours of growth in DMEM (although they are below those of a *crz1* null mutant), which may reflect a rebound from the transient increase in *PMC1* expression that represses accumulation of cytosolic calcium levels. In rich medium (YPD), however, only the *crz1* deletion strain accumulated cytosolic calcium (Figure 9E), which reinforces the idea that Pdr802 acts primarily in host-like conditions.

Since we had observed that Pdr802 regulates at least two targets of calcineurin, we compared gene expression profiles of a calcineurin mutant (55) to our ChIP-Seq data set. Of the 393 genes that were differentially expressed in the calcineurin mutant under thermal stress, 45 were identified in our ChIP-Seq study and. Notably, 8 genes in this group encode transmembrane transporters and 37 contain a Pdr802 binding motif within 1,000 bp of the start site (Data Set S2, Sheet 5).

DISCUSSION

The host lung environment encountered early in infection presents multiple challenges to *C. neoformans* survival, including nutrient limitation, high pH, and oxidative stress (61, 85, 86). Cryptococcal cells lacking Pdr802 are unable to proliferate in this context, and only survive for a few days in tissue culture media. Several factors may contribute to these defects. One may be reduced ability of this mutant to compensate for nutrient limitation, suggested by the multiple membrane transporters implicated as Pdr802 targets by our ChIP-Seq analysis. Because these studies do not indicate the direction in which gene expression is altered, we examined the expression of *PDR802* and its potential targets in published RNA-Seq data sets. We noted that *PDR802* expression in *C. neoformans* cells rises 3-fold upon internalization by macrophages (73),

while its target *HXS1*, which encodes a high affinity glucose transporter, is upregulated 11-fold. *HXS1* expression is known to be induced by glucose limitation, so this is consistent with nutritional deprivation within phagocytes (75). In contrast, the expression of the hexose transporter *HXT1*, normally induced by glucose (74, 75), is downregulated (2.5-fold) in this context (73).

Our measurements of cytosolic calcium show that calcium availability is also modulated by Pdr802. This is likely achieved through its regulation of the calcium transporter Pmc1, demonstrated by our ChIP and qRT-PCR studies. Since calcium ion is a major second messenger in eukaryotic cells, the accumulation of Ca^{2+} in *pdr802* cells could affect multiple processes central to its host interactions, including stress responses and cell wall integrity (59, 60, 80, 83, 87). Pmc1 and at least 38 other genes that are targets of Pdr802 are also downstream targets of calcineurin (55, 61), suggesting that Pdr802 is a downstream effector of calcineurin in the context of host infection. Pmc1 is also regulated by Crz1 (55).

C. neoformans dissemination to the brain is the main driver of patient mortality (2). We found that dissemination of *pdr802* cells is significantly impaired, although they do occasionally reach the brain. These observations can be explained by a combination of factors. First, the limited accumulation of the *pdr802* mutant in the lungs, discussed above, may directly affect dissemination (88). Second, this strain survives poorly in mouse serum, as demonstrated directly by our culture experiments and indirectly by our inability to detect it in the blood of infected mice (even 75 days after infection). This might occur because the cells do not reach the blood or because they are rapidly eliminated, consistent with previous observations (89). Third, the thick capsules of the *pdr802* mutant

reduce its ability to reach the central nervous system. This is true whether fungal brain entry occurs directly, by the movement of free fungi across the BBB, or indirectly, via a Trojan horse mechanism that requires macrophage uptake (12); such uptake is impeded by enlarged capsules, independent of cell size (29). Fourth, inositol transporters, two of which we found to be regulated by Pdr802, are required for normal *C. neoformans* dissemination to the brain (76). Notably, expression of one of these, *ITR2*, is upregulated during *C. neoformans* engulfment by macrophages (2.4-fold), like *PDR802* (3-fold), although the other, *ITR3c*, was not differentially expressed under these conditions (73). Interestingly, despite all of these obstacles to dissemination, cells that do reach the brain are able to proliferate to wild-type levels.

Titan cells are a robust and persistent morphotype of *C. neoformans* that contribute to yeast virulence (43). We showed that cells lacking Pdr802 demonstrate increased formation of Titan cells *in vivo* and *in vitro*, suggesting that this TF is a novel repressor of this process. Although Titan cells enhance aspects of cryptococcal pathogenesis (18, 90), their overproduction negatively impacts dissemination to the brain due to their resistance to phagocytosis by macrophages (18, 43) and decreased penetration of biological barriers (18).

Under conditions of nutrient limitation, such as those encountered during host infection, Pdr802 regulates a variety of transmembrane transporters to moderate the effects of this environment. These conditions also stimulate Titan cell formation (45–47). In the absence of Pdr802, this compensation does not occur, and Titan cell formation increases. Pdr802 may also indirectly regulate Titan cell formation by regulating other TFs that impact this process, such as Zfc3. This protein (also known as Cqs2) is

upregulated during Titan cell formation *in vitro* (46) and is further regulated by Qsp1 (91, 92), a quorum sensing molecule that inhibits Titan cell formation (45, 46).

Our studies *in vitro*, *ex vivo*, and *in vivo* show that Pdr802 downregulates capsule, a feature that is highly induced in the host or host-like conditions and depends on environmental factors that include nutrient availability (93). Capsule thickness could be modulated by Pdr802's repression of the TF Bzp4 (Figure S7B), which is downregulated when *C. neoformans* is engulfed by macrophages (concomitant with *PDR802* upregulation) (73). Our ChIP-Seq results also suggest that Pdr802 interacts with sequences upstream of four other capsule-related transcription factors (Ecm2201, Mln1, Zfc3 and Zfc14) (37, 50). Finally, dysregulation of intracellular calcium concentration also affects capsule production (83).

Our results show that Pdr802 influences key cryptococcal phenotypes that influence virulence, including nutrient acquisition, titanisation, and capsule production. We have further identified multiple genes that are central in these processes and are directly or indirectly regulated by Pdr802. Some of these targets are also regulated by calcineurin (e.g. Had1 and Pmc1) or by another important TF, Gat201 (e.g. Ecm2201, CNAG_05867, CNAG_01552 and CNAG_01040) (58). The expression of *PDR802* itself, along with that of one target, *ITR3C*, is also regulated by another TF, Hob1 (65). The crosstalk between all of these regulatory mechanisms remains to be dissected. Nonetheless, it is evident that Pdr802 is critical for both survival in the lung and dissemination to the brain, thus explaining its role in cryptococcal virulence.

MATERIALS AND METHODS

Strain construction and cell growth

We previously reported the *PDR802* deletion mutant (*pdr802*) in the KN99α strain background (94) that was used in this work (37). Complementation of this mutant with the wild-type gene at the native locus (*PDR802*) and construction of a strain that expresses Pdr802 with N-terminal mCherry (mCherry-Pdr802) are detailed in the Supplementary Methods. For all studies, *C. neoformans* strains were inoculated from single colonies into YPD medium (2% [wt/vol] dextrose, 2% [wt/vol] Bacto peptone and 1% [wt/vol] yeast extract in double-distilled water [ddH_2O]) and grown overnight at 30°C with shaking at 230 rpm before further handling as detailed below. To assess viability during growth in tissue culture medium, overnight cultures were washed with phosphate-buffered saline (PBS), diluted to 10^6 cells/ml in DMEM (Sigma, S6429), plated (1 ml/well) in triplicate in 24-well plates, and incubated at 37°C and 5% CO_2. At the indicated times cells were mixed thoroughly, diluted in PBS, and plated on YPD agar (YPD medium, 2% agar [wt/vol]) for assessment of colony-forming units (CFU). To assess viability during growth in mouse serum, mouse blood was collected as described under “Animal experiments” and YPD-grown cryptococcal cells (10^3) were incubated in 100 µl of serum in 96-well plates for 24 h at 37°C and 5% CO_2 and CFU counted as above.

Animal experiments

All animal protocols were approved by the Washington University Institutional Animal Care and Use Committee (reference 20170131) or Comissão de Ética no Uso de animais – CEUA (reference 30936), and care was taken to minimize handling and discomfort. For survival studies, groups of five 4- to 6-week-old female C57BL/6 mice (The Jackson Laboratory) were anesthetized by subcutaneous injection of 1.20 mg ketamine and 0.24

mg xylazine in 120 µl sterile water and intranasally infected with 5 x 10^4 cryptococcal cells. The mice were monitored and humanely sacrificed when their weight decreased to below 80% of initial weight, at which point organ burden was assessed. The lungs and brains were harvested, homogenized, diluted and plated on YPD agar. The resulting CFU were enumerated and survival differences were assessed by Kaplan-Meier analysis.

For timed organ burden studies, *C. neoformans* overnight cultures were centrifuged (1,000 x *g* for 3 min), washed with sterile PBS, and resuspended in PBS to 1 x 10^6 cells/ml. Groups of three 4- to 6-week-old female C57BL/6 mice (Centro Multidisciplinar para Investigação Biológica na Área da Ciência em Animais de Laboratório, CEMIB) were anesthetized as above and intranasally infected with 5 x 10^4 cryptococcal cells, and monitored as above. At set time points post-infection (see text), mice were sacrificed and fungal burden was assessed from organs (as above) or blood (obtained by cardiac puncture). Organ burden was analyzed by Kruskal-Wallis test with Dunn's multiple comparison *post hoc* test for each day post-infection.

To assess cryptococcal viability in mouse serum, 6 BALB/c mice were anesthetized with isoflurane and blood was collected from the retro-orbital space using a sterile capillary tube. Collected blood was incubated at 37°C for 30 min and serum was isolated by centrifugation at 1,000 x *g* for 15 min and then heat-inactivated at 56 °C for 30 min.

Capsule analysis

To qualitatively assess capsule thickness, strains were grown on YPD medium for 16 h and washed with PBS, and 10^6 cells were incubated in DMEM or mouse serum for 24 h at 37°C and 5% CO_2. After incubation, cells were fixed in 4% paraformaldehyde and washed three times with PBS. *C. neoformans* cells were placed on glass slides and

mixed with similar volumes of India ink and the capsule was measured as previously described (95).

For population-level capsule measurement, *C. neoformans* strains were grown overnight in YPD, washed with PBS, and diluted to 10^6 cells/ml in DMEM. 150 µl aliquots were then plated in quadruplicate in the middle 32 wells of a poly-L-lysine coated 96-well plate (Fisher 655936) and incubated at 37°C and 5% CO_2. After 24 hours, the cells were washed with PBS and incubated with 150 µl of a staining mixture (100 µg/ml Calcofluor white to stain cell walls, 50 µg/ml of the anticapsular monoclonal antibody 302 conjugated to Alexa Fluor 488 (Molecular probes), and 1.5% goat serum in PBS) for 30 minutes at room temperature in the dark. The cells were washed again with PBS, fixed with 4% formaldehyde for 10 minutes at room temperature, washed with PBS, and each well refilled with 150 µl PBS. The cells were imaged using a BioTek Cytation 3 imager, which automatically collected 100 images per well in a grid pattern at the well center. Image files were prepared for analysis with the GE InCell Translator and assembled into .xdce image stacks for analysis with the GE INCell Developer Toolbox 1.9. Cell wall and capsule images were first filtered to remove background noise and border objects and then cells were identified using shape-based object segmentation (3-pixel kernel, 50% sensitivity) followed by watershed clump breaking to prevent apparent connectivity caused by incomplete segmentation. Target linking was performed to assign each cell wall object to one capsule object based on known 1:1 pairing and location, generating a target set. Capsule and cell wall object diameters were calculated for each target set (hundreds to thousands per well), and the difference between each pair of measurements was defined as the capsule thickness. Data were normalized by the difference in capsule thickness between uninduced and induced WT cells, which were included in each

experiment, and compared to hypercapsular (*pkr1*) (37) and hypocapsular (*ada2*) (96) control strains in each experiment. Capsule sizes were compared by One-Way ANOVA with Dunnett's multiple comparison *post hoc* test.

To measure capsule thickness of cryptococcal cells grown in the lungs of infected mice, lung homogenates were filtered through a cell strainer with 40 µm pores using a syringe plunger, fixed in 3.7% formaldehyde, and used for India ink staining and measurement as above. For the visualization of KN99α and *PDR802* cells from mouse lungs after 18 days of infection, the tissue was treated with 50 µg/ml DNAse I for 30 min at 37°C.

GXM immunoblotting was conducted as previously described (69). Briefly, 10^6 cells/ml were grown in DMEM for 24 and 48 h and in CIM (0.17% [wt/vol] yeast nitrogen base without amino acids and ammonium sulfate, 0.15% [wt/vol] asparagine, 2% [wt/vol] glucose, 12 mM $NaHCO_3$, 35 mM MOPS [morpholinepropanesulfonic acid], pH 7.1) medium or YPD for 24 h. Culture supernatant fractions were then resolved by gel electrophoresis on 0.6% agarose, transferred onto nylon membranes, and probed with 1 µg/ml anti-GXM antibody 302 or 18B7.

Phenotypic assays

For stress plates, cryptococcal cells were grown overnight in YPD, washed with PBS, and diluted to 10^7 cells/ml in PBS. Aliquots (3 µl) of 10-fold serial dilutions were spotted on YPD or YNB agar supplemented with various stressors (sorbitol, NaCl, $CaCl_2$, LiCl, Congo Red, Calcofluor white, caffeine, SDS, $NaNO_2$, H_2O_2 and ethanol) in the concentrations indicated in the figures. Melanization was tested on plates made by mixing 10 ml of 2X minimal medium (2 g/L L-asparagine, 1 g/L $MgSO_4 \cdot 7H_2O$, 6 g/L KH_2PO_4, 2 g/L thiamine, 2 mM L-3,4-dihydroxyphenylalanine [L-DOPA] and 0.1%

dextrose was added for melanization induction or 0.5% for melanization inhibition) with 10 ml of 2% agar-water per plate. A control strain lacking the ability to melanize was used as a control (*lac1*) (97). For the solid urease assay, 10 µl of a 10^7 cells/ml suspension in water was plated on Christensen's urea solid media (1 g/L peptone, 1 g/L dextrose, 5 g/L NaCl, 0.8 g/L KH_2PO_4, 1.2 g/L Na_2HPO_4, 0.012 g/L phenol red and 15 g/L agar, pH 6.8). Plates were incubated at 30°C or 37°C.

Titan cells

Titan cell induction was performed in 1x PBS supplemented with 10% heat inactivated Fetal Calf Serum (FCS) for 72 hours at 37°C and 5% CO_2 as recently described (47) and quantified by flow cytometry as previously reported (45, 46).

Phagocytosis

J774.16 cells were prepared for uptake experiments by seeding (10^5 cells/well) in a 96-well plate and incubating in DMEM supplemented with 10% Fetal Bovine Serum (FBS) at 37°C and 5% CO_2 for 24 h. *C. neoformans* cells were prepared for uptake experiments by inoculating an overnight culture in YPD into either DMEM or Titan cell induction medium (47) and growing at 37°C and 5% CO_2 for 24 or 72 h, respectively. To initiate the study, cryptococcal cells were washed with PBS and opsonized with anti-capsular antibody 18B7 (1 µg/ml) for 1 h at 37°C while macrophages were activated with 50 nM phorbol myristate acetate (PMA) for 1 h at 37°C and 5% CO_2; 10^6 cryptococcal cells were then incubated with the macrophages for 2 h at 37°C and 5% CO_2. The wells were then washed three times with warm PBS and the macrophages lysed with 0.1% Triton in PBS and plated for CFU as above. Fold-change in CFU was assessed by comparison to the CFU of opsonized cells. One-Way ANOVA with Dunnett's multiple comparison *post hoc*

test was used to compare phagocytosis of *pdr802* and *PDR802* strains with that of KN99α.

Chromatin Immunoprecipitation (ChIP)

ChIP studies were performed as previously described (37, 96). Briefly, wild type and N-terminal-mCherry-Pdr802 strains were cultivated in DMEM for 24 hours at 37°C and 5% CO_2. The cells were then fixed with formaldehyde, lysed by mechanical bead-beating, and the cell debris removed by centrifugation. The supernatant fraction was sheared by sonication, centrifuged, and an aliquot was reserved as 'Input'. The remaining material was incubated with rabbit IgG anti-mCherry antibody (Abcam, ab213511) tethered to protein A sepharose ('IP') or sepharose alone ('Mock') overnight at 4°C. The beads were then washed, incubated at 65°C to reverse DNA-DNA and DNA-protein crosslinks and the DNA recovered by phenol/chloroform/isoamyl alcohol (25:24:1) extraction, ethanol precipitation, and resuspension in nuclease-free water.

Samples were submitted to the Washington University Genome Technology Access Center for library preparation and DNA samples were sequenced using the Illumina Nextseq platform. The first replicate was sequenced using paired-end 2x75-bp reads and replicates 2 and 3 were sequenced using single-end 75-bp reads; the minimum coverage obtained was ~16x. The quality of the reads was evaluated by FastQC (98). Fastq files were aligned to the KN99 genome (99) using NextGenMap 0.5.3 (100). SAM files were converted to bam, reads were sorted and indexed, and read duplicates were removed from the final bam files using samtools (101). Samtools was also used to filter out reads with a mapping quality lesser than 20 phreds to guarantee single alignment of the reads. Peaks were called using MACS2 (2.1.1.20160309) (102), filtered by size (maximum

threshold 5 kb and no minimum), and annotated using Homer 4.8 (103). The significant peaks were chosen using the cutoff of fold enrichment above 2 and adjusted $p < 0.05$. The Pdr802 binding motif was defined using DREME (72) and Gene Ontology was performed using Revigo (104). The read coverage of each peak was obtained using Samtools (101).

qRT-PCR

RNA from wild-type and *pdr802* cells grown in DMEM at 37°C with 5% CO_2 for 3 or 24 hours was extracted with TriZol® reagent (Invitrogen, MA, USA) according to the manufacturer's instructions. RNA integrity was assessed by electrophoresis on 1% agarose and quantification was performed by absorbance analysis using a NanoDrop™ 2000 spectrophotometer (Thermo Fisher Scientific). cDNAs were prepared from DNase (Promega, WI, USA)-treated total RNA samples (290 ng) using ImProm-II reverse transcriptase (Promega) and oligo-dT. Quantitative real-time PCR (qRT-PCR) was performed on a Fast 7500 real-time PCR system (Applied Biosystems, MA, USA) with the following thermal cycling conditions: 95°C for 10 min followed by 50 cycles of 95°C for 15 s, 55°C for 15 s, and 60°C for 60 s. Platinum® SYBR® green qPCR Supermix (Invitrogen) was used as the reaction mix and supplemented with 5 pmol of each primer (see Data Set S2, Sheet 6, for sequences) and 8 ng of cDNA template for a final volume of 20 µl. All experiments were performed in biological triplicate and each sample was analyzed in triplicate for each primer pair. Melting curve analysis was performed at the end of the reaction to confirm the presence of a single PCR product. Data were normalized to levels of *ACT1*, which was included in each set of PCR experiments. Relative expression was determined using the $2^{-\Delta Ct}$ method.

Intracellular calcium measurement

To measure intracellular free Ca^{2+}, yeast cells were cultured overnight in YPD at 30°C with shaking, washed three times with deionized water, diluted to 10^6 cells/ml in DMEM (Sigma, S6429), plated (1 ml/well) in triplicate in 24-well plates, and incubated at 37°C and 5% CO_2 for 24 hours. At the indicated times, cells were mixed thoroughly, diluted in PBS containing 2 μM Fluo4-AM (ThermoFisher), incubated at 30°C for 30 min, and analysed using flow cytometry. The overnight culture was used as a control and treated as above.

Data availability

Data is available at the NCBI Gene Expression Omnibus (accession number GSE153134).

REFERENCES

1. Kwon-Chung KJ, Fraser JA, Doering TL, Wang ZA, Janbon G, Idnurm A, Bahn Y-S. 2014. *Cryptococcus neoformans* and *Cryptococcus gattii*, the Etiologic Agents of Cryptococcosis. Cold Spring Harb Perspect Med 4:a019760.

2. Rajasingham R, Smith RM, Park BJ, Jarvis JN, Govender NP, Chiller TM, Denning DW, Loyse A, Boulware DR. 2017. Global burden of disease of HIV-associated cryptococcal meningitis: an updated analysis. Lancet Infect Dis 17:873–881.

3. Ballou ER, Johnston SA. 2017. The cause and effect of *Cryptococcus* interactions with the host. Curr Opin Microbiol 40:88–94.

4. Sabiiti W, May RC. 2012. Mechanisms of infection by the human fungal pathogen *Cryptococcus neoformans*. Future Microbiol 7:1297–1313.

5. Chang YC, Stins MF, McCaffery MJ, Miller GF, Pare DR, Dam T, Paul-Satyasee M, Kim KS, Kwon-Chung KJ. 2004. Cryptococcal yeast cells invade the central nervous system via transcellular penetration of the blood-brain barrier. Infect Immun 72:4985–4995.

6. Huang S-H, Long M, Wu C-H, Kwon-Chung KJ, Chang YC, Chi F, Lee S, Jong A. 2011. Invasion of *Cryptococcus neoformans* into Human Brain Microvascular Endothelial Cells Is Mediated through the Lipid Rafts-Endocytic Pathway via the Dual Specificity Tyrosine Phosphorylation-regulated Kinase 3 (DYRK3). J Biol Chem 286:34761–34769.

7. Jong A, Wu C-H, Shackleford GM, Kwon-Chung KJ, Chang YC, Chen H-M, Ouyang Y, Huang S-H. 2008. Involvement of human CD44 during *Cryptococcus neoformans* infection of brain microvascular endothelial cells. Cell Microbiol 10:1313–1326.

8. Maruvada R, Zhu L, Pearce D, Zheng Y, Perfect J, Kwon-Chung KJ, Kim KS. 2012. *Cryptococcus neoformans* phospholipase B1 activates host cell Rac1 for traversal across the blood-brain barrier. Cell Microbiol 14:1544–1553.

9. Chen SHM, Stins MF, Huang S-H, Chen YH, Kwon-Chung KJ, Chang Y, Kim KS, Suzuki K, Jong AY. 2003. *Cryptococcus neoformans* induces alterations in the cytoskeleton of human brain microvascular endothelial cells. J Med Microbiol 52:961–970.

10. Olszewski MA, Noverr MC, Chen G-H, Toews GB, Cox GM, Perfect JR, Huffnagle GB. 2004. Urease Expression by *Cryptococcus neoformans* Promotes Microvascular Sequestration, Thereby Enhancing Central Nervous System Invasion. Am J Pathol 164:1761–1771.

11. Shi M, Li SS, Zheng C, Jones GJ, Kim KS, Zhou H, Kubes P, Mody CH. 2010. Real-time imaging of trapping and urease-dependent transmigration of *Cryptococcus neoformans* in mouse brain. J Clin Invest 120:1683–1693.

12. Santiago-Tirado FH, Onken MD, Cooper JA, Klein RS, Doering TL. 2017. Trojan Horse Transit Contributes to Blood-Brain Barrier Crossing of a Eukaryotic Pathogen. MBio 8:e02183-16.

13. Jarvis JN, Bicanic T, Loyse A, Namarika D, Jackson A, Nussbaum JC, Longley N, Muzoora C, Phulusa J, Taseera K, Kanyembe C, Wilson D, Hosseinipour MC, Brouwer AE, Limmathurotsakul D, White N, van der Horst C, Wood R, Meintjes G, Bradley J, Jaffar S, Harrison T. 2014. Determinants of Mortality in a Combined Cohort of 501 Patients With HIV-Associated Cryptococcal Meningitis: Implications for Improving Outcomes. Clin Infect Dis 58:736–745.

14. John R. Perfect, William E. Dismukes, Francoise Dromer, David L. Goldman, John R. Graybill, Richard J. Hamill, Thomas S. Harrison, Robert A. Larsen, Olivier Lortholary, Minh-Hong Nguyen, Peter G. Pappas, William G. Powderly, Nina Singh, Jack D. Sobel TCS. 2010. Clinical Practice Guidelines for the Management of Cryptococcal Disease: 2010 Update by the Infectious Diseases Society of America. Chinese J Infect Chemother 50:291–322.

15. Nosanchuk JD, Casadevall A. 2003. The contribution of melanin to microbial

pathogenesis. Cell Microbiol 5:203–223.

16. Singh A, Panting RJ, Varma A, Saijo T, Waldron KJ, Jong A, Ngamskulrungroj P, Chang YC, Rutherford JC, Kwon-Chung KJ. 2013. Factors Required for Activation of Urease as a Virulence Determinant in *Cryptococcus neoformans*. MBio 4:e00220-13.

17. Chang YC, Kwon-Chung KJ. 1994. Complementation of a capsule-deficient mutation of *Cryptococcus neoformans* restores its virulence. Mol Cell Biol 14:4912–4919.

18. Okagaki LH, Strain AK, Nielsen JN, Charlier C, Baltes NJ, Chrétien F, Heitman J, Dromer F, Nielsen K. 2010. Cryptococcal Cell Morphology Affects Host Cell Interactions and Pathogenicity. PLoS Pathog 6:e1000953.

19. Zaragoza O, Nielsen K. 2013. Titan cells in *Cryptococcus neoformans*: cells with a giant impact. Curr Opin Microbiol 16:409–413.

20. Wang Y, Aisen P, Casadevall A. 1995. *Cryptococcus neoformans* melanin and virulence: Mechanism of action. Infect Immun 63:3131–3136.

21. Mednick AJ, Nosanchuk JD, Casadevall A. 2005. Melanization of *Cryptococcus neoformans* Affects Lung Inflammatory Responses during Cryptococcal Infection. Infect Immun 73:2012–2019.

22. Wang Y, Casadevall A. 1994. Susceptibility of melanized and nonmelanized *Cryptococcus neoformans* to nitrogen- and oxygen-derived oxidants. Infect Immun 62:3004–7.

23. Doering TL, Nosanchuk JD, Roberts WK, Casadevall A. 1999. Melanin as a

potential cryptococcal defence against microbicidal proteins. Med Mycol 37:175–81.

24. Cox GM, Mukherjee J, Cole GT, Casadevall A, Perfect JR. 2000. Urease as a virulence factor in experimental cryptococcosis. Infect Immun 68:443–8.

25. Bose I, Reese AJ, Ory JJ, Janbon G, Doering TL. 2003. A Yeast under Cover: the Capsule of *Cryptococcus neoformans*. Eukaryot Cell 2:655–663.

26. Wang ZA, Li LX, Doering TL. 2018. Unraveling synthesis of the cryptococcal cell wall and capsule. Glycobiology 28:719–730.

27. Agustinho DP, Miller LC, Li LX, Doering TL. 2018. Peeling the onion: the outer layers of *Cryptococcus neoformans*. Mem Inst Oswaldo Cruz 113:e180040.

28. Bulmer GS, Sans MD. 1967. *Cryptococcus neoformans*. II. Phagocytosis by human leukocytes. J Bacteriol 94:1480–3.

29. Bulmer GS, Sans MD. 1968. *Cryptococcus neoformans*. 3. Inhibition of phagocytosis. 95:5–8.

30. Tacker JR, Farhi F, Bulmer GS. 1972. Intracellular fate of *Cryptococcus neoformans*. Infect Immun 6:162–7.

31. Monari C, Bistoni F, Vecchiarelli A. 2006. Glucuronoxylomannan exhibits potent immunosuppressive properties. FEMS Yeast Res 6:537–542.

32. Hayes JB, Sircy LM, Heusinkveld LE, Ding W, Leander RN, McClelland EE, Nelson DE. 2016. Modulation of Macrophage Inflammatory Nuclear Factor κB (NF-κB) Signaling by Intracellular *Cryptococcus neoformans*. J Biol Chem 291:15614–

15627.

33. Fonseca FL, Nohara LL, Cordero RJB, Frases S, Casadevall A, Almeida IC, Nimrichter L, Rodrigues ML. 2010. Immunomodulatory Effects of Serotype B Glucuronoxylomannan from *Cryptococcus gattii* Correlate with Polysaccharide Diameter. Infect Immun 78:3861–3870.

34. Garcia-Hermoso D, Dromer F, Janbon G. 2004. *Cryptococcus neoformans* Capsule Structure Evolution *In Vitro* and during Murine Infection. Infect Immun 72:3359–3365.

35. Guimarães AJ, Frases S, Cordero RJB, Nimrichter L, Casadevall A, Nosanchuk JD. 2010. *Cryptococcus neoformans* responds to mannitol by increasing capsule size *in vitro* and *in vivo*. Cell Microbiol 12:740–753.

36. Cordero RJB, Pontes B, Guimarães AJ, Martinez LR, Rivera J, Fries BC, Nimrichter L, Rodrigues ML, Viana NB, Casadevall A. 2011. Chronological Aging Is Associated with Biophysical and Chemical Changes in the Capsule of *Cryptococcus neoformans*. Infect Immun 79:4990–5000.

37. Maier EJ, Haynes BC, Gish SR, Wang ZA, Skowyra ML, Marulli AL, Doering TL, Brent MR. 2015. Model-driven mapping of transcriptional networks reveals the circuitry and dynamics of virulence regulation. Genome Res 25:690–700.

38. Silveira CP, Piffer AC, Kmetzsch L, Fonseca FL, Soares DA, Staats CC, Rodrigues ML, Schrank A, Vainstein MH. 2013. The heat shock protein (Hsp) 70 of *Cryptococcus neoformans* is associated with the fungal cell surface and influences the interaction between yeast and host cells. Fungal Genet Biol 60:53–63.

39. Santos JRA, Holanda RA, Frases S, Bravim M, Araujo GDS, Santos PC, Costa MC, Ribeiro MJA, Ferreira GF, Baltazar LM, Miranda AS, Oliveira DB, Santos CMA, Fontes ACL, Gouveia LF, Resende-Stoianoff MA, Abrahão JS, Teixeira AL, Paixão TA, Souza DG, Santos DA. 2014. Fluconazole Alters the Polysaccharide Capsule of *Cryptococcus gattii* and Leads to Distinct Behaviors in Murine Cryptococcosis. PLoS One 9:e112669.

40. Alspaugh JA. 2015. Virulence mechanisms and *Cryptococcus neoformans* pathogenesis. Fungal Genet Biol 78:55–58.

41. García-Rodas R, de Oliveira H, Trevijano-Contador N, Zaragoza O. 2018. Cryptococcal Titan Cells: When Yeast Cells Are All Grown up, p. 101–120. *In* Current Topics in Microbiology and Immunology. Springer Verlag.

42. Zhou X, Ballou ER. 2018. The *Cryptococcus neoformans* Titan Cell: From *In Vivo* Phenomenon to *In Vitro* Model. Curr Clin Microbiol Reports 5:252–260.

43. Zaragoza O, García-Rodas R, Nosanchuk JD, Cuenca-Estrella M, Rodríguez-Tudela JL, Casadevall A. 2010. Fungal Cell Gigantism during Mammalian Infection. PLoS Pathog 6:e1000945.

44. Gerstein AC, Fu MS, Mukaremera L, Li Z, Ormerod KL, Fraser JA, Berman J, Nielsen K. 2015. Polyploid Titan Cells Produce Haploid and Aneuploid Progeny To Promote Stress Adaptation. MBio 6:e01340-15.

45. Hommel B, Mukaremera L, Cordero RJBB, Coelho C, Desjardins CA, Sturny-Leclère A, Janbon G, Perfect JR, Fraser JA, Casadevall A, Cuomo CA, Dromer F, Nielsen K, Alanio A. 2018. Titan cells formation in *Cryptococcus neoformans* is

finely tuned by environmental conditions and modulated by positive and negative genetic regulators. PLOS Pathog 14:e1006982.

46. Trevijano-Contador N, de Oliveira HC, García-Rodas R, Rossi SA, Llorente I, Zaballos Á, Janbon G, Ariño J, Zaragoza Ó. 2018. *Cryptococcus neoformans* can form titan-like cells *in vitro* in response to multiple signals. PLOS Pathog 14:e1007007.

47. Dambuza IM, Drake T, Chapuis A, Zhou X, Correia J, Taylor-Smith L, LeGrave N, Rasmussen T, Fisher MC, Bicanic T, Harrison TS, Jaspars M, May RC, Brown GD, Yuecel R, MacCallum DM, Ballou ER. 2018. The *Cryptococcus neoformans* Titan cell is an inducible and regulated morphotype underlying pathogenesis. PLOS Pathog 14:e1006978.

48. García-Barbazán I, Trevijano-Contador N, Rueda C, de Andrés B, Pérez-Tavárez R, Herrero-Fernández I, Gaspar ML, Zaragoza O. 2016. The formation of titan cells in *Cryptococcus neoformans* depends on the mouse strain and correlates with induction of Th2-type responses. Cell Microbiol 18:111–124.

49. Mukaremera L, Lee KK, Wagener J, Wiesner DL, Gow NAR, Nielsen K. 2018. Titan cell production in *Cryptococcus neoformans* reshapes the cell wall and capsule composition during infection. Cell Surf 1:15–24.

50. Jung K-W, Yang D-H, Maeng S, Lee K-T, So Y-S, Hong J, Choi J, Byun H-J, Kim H, Bang S, Song M-H, Lee J-W, Kim MS, Kim S-Y, Ji J-H, Park G, Kwon H, Cha S, Meyers GL, Wang LL, Jang J, Janbon G, Adedoyin G, Kim T, Averette AK, Heitman J, Cheong E, Lee Y-H, Lee Y-W, Bahn Y-S. 2015. Systematic functional profiling of transcription factor networks in *Cryptococcus neoformans*. Nat Commun

6:6757.

51. Schneider R de O, Fogaça N de SS, Kmetzsch L, Schrank A, Vainstein MH, Staats CC. 2012. Zap1 Regulates Zinc Homeostasis and Modulates Virulence in *Cryptococcus gattii*. PLoS One 7:e43773.

52. Garcia-Santamarina S, Festa RA, Smith AD, Yu C-H, Probst C, Ding C, Homer CM, Yin J, Noonan JP, Madhani H, Perfect JR, Thiele DJ. 2018. Genome-wide analysis of the regulation of Cu metabolism in *Cryptococcus neoformans*. Mol Microbiol 108:473–494.

53. Lev S, Kaufman-Francis K, Desmarini D, Juillard PG, Li C, Stifter SA, Feng CG, Sorrell TC, Grau GER, Bahn Y-S, Djordjevic JT. 2017. Pho4 Is Essential for Dissemination of *Cryptococcus neoformans* to the Host Brain by Promoting Phosphate Uptake and Growth at Alkaline pH. mSphere 2:e00381-16.

54. Jung WH, Sham A, White R, Kronstad JW. 2006. Iron Regulation of the Major Virulence Factors in the AIDS-Associated Pathogen *Cryptococcus neoformans*. PLoS Biol 4:e410.

55. Chow EWL, Clancey SA, Billmyre RB, Averette AF, Granek JA, Mieczkowski P, Cardenas ME, Heitman J. 2017. Elucidation of the calcineurin-Crz1 stress response transcriptional network in the human fungal pathogen *Cryptococcus neoformans*. PLOS Genet 13:e1006667.

56. O'Meara TR, Norton D, Price MS, Hay C, Clements MF, Nichols CB, Alspaugh JA. 2010. Interaction of *Cryptococcus neoformans* Rim101 and Protein Kinase A Regulates Capsule. PLoS Pathog 6:e1000776.

57. Gish SR, Maier EJ, Haynes BC, Santiago-Tirado FH, Srikanta DL, Ma CZ, Li LX, Williams M, Crouch EC, Khader SA, Brent MR, Doering TL. 2016. Computational Analysis Reveals a Key Regulator of Cryptococcal Virulence and Determinant of Host Response. MBio 7:e00313-16.

58. Chun CD, Brown JCS, Madhani HD. 2011. A Major Role for Capsule-Independent Phagocytosis-Inhibitory Mechanisms in Mammalian Infection by *Cryptococcus neoformans*. Cell Host Microbe 9:243–251.

59. Moranova Z, Virtudazo E, Hricova K, Ohkusu M, Kawamoto S, Husickova V, Raclavsky V. 2014. The CRZ1/SP1-like gene links survival under limited aeration, cell integrity and biofilm formation in the pathogenic yeast *Cryptococcus neoformans*. Biomed Pap 158:212–220.

60. Lev S, Desmarini D, Chayakulkeeree M, Sorrell TC, Djordjevic JT. 2012. The Crz1/Sp1 Transcription Factor of *Cryptococcus neoformans* Is Activated by Calcineurin and Regulates Cell Wall Integrity. PLoS One 7:e51403.

61. Park H-S, Chow EWL, Fu C, Soderblom EJ, Moseley MA, Heitman J, Cardenas ME. 2016. Calcineurin Targets Involved in Stress Survival and Fungal Virulence. PLOS Pathog 12:e1005873.

62. Lee D, Jang E-H, Lee M, Kim S-W, Lee Y, Lee K-T, Bahn Y-S. 2019. Unraveling Melanin Biosynthesis and Signaling Networks in *Cryptococcus neoformans*. MBio 10:e02267-19.

63. Rhodes J, Desjardins CA, Sykes SM, Beale MA, Vanhove M, Sakthikumar S, Chen Y, Gujja S, Saif S, Chowdhary A, Lawson DJ, Ponzio V, Colombo AL, Meyer W,

Engelthaler DM, Hagen F, Illnait-Zaragozi MT, Alanio A, Vreulink J-M, Heitman J, Perfect JR, Litvintseva AP, Bicanic T, Harrison TS, Fisher MC, Cuomo CA. 2017. Tracing Genetic Exchange and Biogeography of *Cryptococcus neoformans* var. *grubii* at the Global Population Level. Genetics 207:327–346.

64. Liu OW, Chun CD, Chow ED, Chen C, Madhani HD, Noble SM. 2008. Systematic Genetic Analysis of Virulence in the Human Fungal Pathogen *Cryptococcus neoformans*. Cell 135:174–188.

65. Lee K-T, Hong J, Lee D-G, Lee M, Cha S, Lim Y-G, Jung K-W, Hwangbo A, Lee Y, Yu S-J, Chen Y-L, Lee J-S, Cheong E, Bahn Y-S. 2020. Fungal kinases and transcription factors regulating brain infection in *Cryptococcus neoformans*. Nat Commun 11:1521.

66. Krysan DJ, Zhai B, Beattie SR, Misel KM, Wellington M, Lin X. 2019. Host Carbon Dioxide Concentration Is an Independent Stress for *Cryptococcus neoformans* That Affects Virulence and Antifungal Susceptibility. MBio 10:e01410-19.

67. D'Souza CA, Alspaugh JA, Yue C, Harashima T, Cox GM, Perfect JR, Heitman J. 2001. Cyclic AMP-Dependent Protein Kinase Controls Virulence of the Fungal Pathogen *Cryptococcus neoformans*. Mol Cell Biol 21:3179–3191.

68. Hu G, Steen BR, Lian T, Sham AP, Tam N, Tangen KL, Kronstad JW. 2007. Transcriptional Regulation by Protein Kinase A in *Cryptococcus neoformans*. PLoS Pathog 3:e42.

69. Yoneda A, Doering TL. 2008. Regulation of *Cryptococcus neoformans* Capsule Size Is Mediated at the Polymer Level. Eukaryot Cell 7:546–549.

70. McFadden DC, Fries BC, Wang F, Casadevall A. 2007. Capsule Structural Heterogeneity and Antigenic Variation in *Cryptococcus neoformans*. Eukaryot Cell 6:1464–1473.

71. McFadden DC, De Jesus M, Casadevall A. 2006. The Physical Properties of the Capsular Polysaccharides from *Cryptococcus neoformans* Suggest Features for Capsule Construction. J Biol Chem 281:1868–1875.

72. Bailey TL. 2011. DREME: Supp. Bioinformatics 27:1653–1659.

73. Derengowski L da S, Paes HC, Albuquerque P, Tavares AHFP, Fernandes L, Silva-Pereira I, Casadevall A. 2013. The Transcriptional Response of *Cryptococcus neoformans* to Ingestion by *Acanthamoeba castellanii* and Macrophages Provides Insights into the Evolutionary Adaptation to the Mammalian Host. Eukaryot Cell 12:761–774.

74. Chikamori M, Fukushima K. 2005. A new hexose transporter from *Cryptococcus neoformans*: Molecular cloning and structural and functional characterization. Fungal Genet Biol 42:646–655.

75. Liu T-B, Wang Y, Baker GM, Fahmy H, Jiang L, Xue C. 2013. The Glucose Sensor-Like Protein Hxs1 Is a High-Affinity Glucose Transporter and Required for Virulence in *Cryptococcus neoformans*. PLoS One 8:e64239.

76. Liu T-B, Kim J-C, Wang Y, Toffaletti DL, Eugenin E, Perfect JR, Kim KJ, Xue C. 2013. Brain Inositol Is a Novel Stimulator for Promoting *Cryptococcus* Penetration of the Blood-Brain Barrier. PLoS Pathog 9:e1003247.

77. Xue C, Liu T, Chen L, Li W, Liu I, Kronstad JW, Seyfang A, Heitman J. 2010. Role

of an Expanded Inositol Transporter Repertoire in *Cryptococcus neoformans* Sexual Reproduction and Virulence. MBio 1:e.00084-10.

78. Lee K-T, So Y-S, Yang D-H, Jung K-W, Choi J, Lee D-G, Kwon H, Jang J, Wang LL, Cha S, Meyers GL, Jeong E, Jin J-H, Lee Y, Hong J, Bang S, Ji J-H, Park G, Byun H-J, Park SW, Park Y-M, Adedoyin G, Kim T, Averette AF, Choi J-S, Heitman J, Cheong E, Lee Y-H, Bahn Y-S. 2016. Systematic functional analysis of kinases in the fungal pathogen *Cryptococcus neoformans*. Nat Commun 7:12766.

79. Kozubowski L, Lee SC, Heitman J. 2009. Signalling pathways in the pathogenesis of *Cryptococcus*. Cell Microbiol 11:370–380.

80. Fox DS, Cruz MC, Sia RAL, Ke H, Cox GM, Cardenas ME, Heitman J. 2001. Calcineurin regulatory subunit is essential for virulence and mediates interactions with FKBP12-FK506 in *Cryptococcus neoformans*. Mol Microbiol 39:835–849.

81. Odom A. 1997. Calcineurin is required for virulence of *Cryptococcus neoformans*. EMBO J 16:2576–2589.

82. Jung W-H, Son Y-E, Oh S-H, Fu C, Kim HS, Kwak J-H, Cardenas ME, Heitman J, Park H-S. 2018. Had1 Is Required for Cell Wall Integrity and Fungal Virulence in *Cryptococcus neoformans*. Genes|Genomes|Genetics 8:643–652.

83. Kmetzsch L, Staats CC, Cupertino JB, Fonseca FL, Rodrigues ML, Schrank A, Vainstein MH. 2013. The calcium transporter Pmc1 provides Ca 2+ tolerance and influences the progression of murine cryptococcal infection. FEBS J 280:4853–4864.

84. Squizani ED, Oliveira NK, Reuwsaat JCV, Marques BM, Lopes W, Gerber AL, de

Vasconcelos ATR, Lev S, Djordjevic JT, Schrank A, Vainstein MH, Staats CC, Kmetzsch L. 2018. Cryptococcal dissemination to the central nervous system requires the vacuolar calcium transporter Pmc1. Cell Microbiol 20:e12803.

85. Chang AL, Kang Y, Doering TL. 2019. Cdk8 and Ssn801 Regulate Oxidative Stress Resistance and Virulence in *Cryptococcus neoformans*. MBio 10:e02818-18.

86. Watkins R, King J, Johnston S. 2017. Nutritional Requirements and Their Importance for Virulence of Pathogenic *Cryptococcus* Species. Microorganisms 5:65.

87. Cruz MC. 2001. Calcineurin is required for hyphal elongation during mating and haploid fruiting in *Cryptococcus neoformans*. EMBO J 20:1020–1032.

88. Denham S, Brown J. 2018. Mechanisms of Pulmonary Escape and Dissemination by *Cryptococcus neoformans*. J Fungi 4:25.

89. Sun D, Sun P, Li H, Zhang M, Liu G, Strickland AB, Chen Y, Fu Y, Xu J, Yosri M, Nan Y, Zhou H, Zhang X, Shi M. 2019. Fungal dissemination is limited by liver macrophage filtration of the blood. Nat Commun 10:4566.

90. Okagaki LH, Nielsen K. 2012. Titan Cells Confer Protection from Phagocytosis in *Cryptococcus neoformans* Infections. Eukaryot Cell 11:820–826.

91. Summers DK, Perry DS, Rao B, Madhani HD. 2020. Coordinate genomic association of transcription factors controlled by an imported quorum sensing peptide in *Cryptococcus neoformans*. bioRxiv 2020.03.30.016329.

92. Tian X, He G-J, Hu P, Chen L, Tao C, Cui Y-L, Shen L, Ke W, Xu H, Zhao Y, Xu Q, Bai F, Wu B, Yang E, Lin X, Wang L. 2018. *Cryptococcus neoformans* sexual

reproduction is controlled by a quorum sensing peptide. Nat Microbiol 3:698–707.

93. Srikanta D, Santiago-Tirado FH, Doering TL. 2014. *Cryptococcus neoformans* : historical curiosity to modern pathogen. Yeast 31:47–60.

94. Nielsen K, Cox GM, Wang P, Toffaletti DL, Perfect JR, Heitman J. 2003. Sexual Cycle of *Cryptococcus neoformans* var. *grubii* and Virulence of Congenic a and α Isolates. Infect Immun 71:4831–4841.

95. Reuwsaat JCV, Motta H, Garcia AWA, Vasconcelos CB, Marques BM, Oliveira NK, Rodrigues J, Ferrareze PAG, Frases S, Lopes W, Barcellos VA, Squizani ED, Horta JA, Schrank A, Rodrigues ML, Staats CC, Vainstein MH, Kmetzsch L. 2018. A Predicted Mannoprotein Participates in *Cryptococcus gattii* Capsular Structure. mSphere 3: e00023-18.

96. Haynes BC, Skowyra ML, Spencer SJ, Gish SR, Williams M, Held EP, Brent MR, Doering TL. 2011. Toward an Integrated Model of Capsule Regulation in *Cryptococcus neoformans*. PLoS Pathog 7:e1002411.

97. Walton FJ, Idnurm A, Heitman J. 2005. Novel gene functions required for melanization of the human pathogen *Cryptococcus neoformans*. Mol Microbiol 57:1381–1396.

98. Babraham Bioinformatics - FastQC A Quality Control tool for High Throughput Sequence Data.

99. Friedman RZ, Gish SR, Brown H, Brier L, Howard N, Doering TL, Brent MR. 2018. Unintended Side Effects of Transformation Are Very Rare in *Cryptococcus neoformans*. Genes|Genomes|Genetics 8:815–822.

100. Sedlazeck FJ, Rescheneder P, von Haeseler A. 2013. NextGenMap: fast and accurate read mapping in highly polymorphic genomes. Bioinformatics 29:2790–1.

101. Li H, Handsaker B, Wysoker A, Fennell T, Ruan J, Homer N, Marth G, Abecasis G, Durbin R, 1000 Genome Project Data Processing Subgroup. 2009. The Sequence Alignment/Map format and SAMtools. Bioinformatics 25:2078–2079.

102. Zhang Y, Liu T, Meyer CA, Eeckhoute J, Johnson DS, Bernstein BE, Nussbaum C, Myers RM, Brown M, Li W, Liu XS. 2008. Model-based Analysis of ChIP-Seq (MACS). Genome Biol 9:R137.

103. Heinz S, Benner C, Spann N, Bertolino E, Lin YC, Laslo P, Cheng JX, Murre C, Singh H, Glass CK. 2010. Simple combinations of lineage-determining transcription factors prime cis-regulatory elements required for macrophage and B cell identities. Mol Cell 38:576–89.

104. Supek F, Bošnjak M, Škunca N, Šmuc T. 2011. REVIGO Summarizes and Visualizes Long Lists of Gene Ontology Terms. PLoS One 6:e21800.

105. Li LX, Rautengarten C, Heazlewood JL, Doering TL. 2018. Xylose donor transport is critical for fungal virulence. PLOS Pathog 14:e1006765.

ACKNOWLEDGMENTS

We appreciate helpful discussions with Michael Brent, Charley Christian Staats, and members of the Doering, Kmetzsch and Brent labs. We are grateful to Thomas Hurtaux, Eamim Squizani, and Julia Sperotto for assistance with mouse experiments, Guohua Chen for helping with spotting assays, and Jessica Plaggenberg for assistance with

library preparation and sequencing. We thank Marilene Henning Vainstein and her lab for providing support with *in vivo* experiments. We also thank Liza Miller for comments on the manuscript and Arturo Casadevall for providing the antibody anti-GXM (18B7).

These studies were supported by National Institutes of Health grants AI087794, AI36688, and AI140979 to TLD and grants from Coordenação de Aperfeiçoamento de Pessoal de Nível Superior (CAPES, Brazil), Conselho Nacional de Desenvolvimento Científico e Tecnológico (CNPq, Brazil – Grant number 310510/2018-0), and Fundação de Amparo à Pesquisa do Estado do Rio Grande do Sul (FAPERGS, Brazil) to LK. CAPES fully supported JCVR during her studies in Brazil; her studies in the United States were partially supported by this source (Advanced Network of Computational Biology - RABICÓ - Biocomputational Grant 23038.010041/2013-13).

AUTHORS CONTRIBUTION

Conceived and designed the experiments: J.C.V.R., A.L.C., L.K. and T.L.D.;

Performed the experiments: J.C.V.R., H.M., H.B., and A.L.C;

Analyzed the data: J.C.V.R., A.L.C., D.P.A., L.K. and T.L.D.;

Contributed reagents and materials: L.K. and T.L.D.;

Wrote the paper: J.C.V.R, L.K. and T.L.D.

COMPETING INTERESTS

The authors declare no competing financial interests.

FIGURE LEGENDS

Figure 1. The transcription factor Pdr802 influences *C. neoformans* virulence. A. Survival of C57BL/6 mice over time after intranasal inoculation with 5 x 10^4 cryptococci, with sacrifice triggered by weight below 80% of peak. B. Mean +/- SD of total colony-forming units (CFU) in lung tissue at various times post-infection. CFU inoculated for each strain were 41,400 (KN99α), 42,800 (*pdr802*) and 26,600 (*PDR802*). $p<0.05$ for *pdr802* compared to the other strains at all time points.

Figure 2. *PDR802* expression is required for cell viability and induced during growth in host-like conditions. A. Cells grown in DMEM at 37°C and 5% CO_2 were sampled at the times indicated and plated on YPD to assess viability (measured by CFU and plotted as fold-change from time 0). B. *PDR802* expression in KN99α cells grown in DMEM at 37°C and 5% CO_2 was assessed by RNA-seq as in Li *et al*., 2018 (105).

Figure 3. The *pdr802* mutant is hypercapsular. A. Representative immunofluorescence micrographs of the indicated strains after growth in DMEM (37°C, 5% CO_2) for 24 hours. The capsule was stained with monoclonal antibody anti-GXM 302 conjugated with Alexa 488 (green) and the cell wall with Calcofluor White (blue). All images are to the same scale; scale bar, 5 µm. B. Capsule thickness distribution for the indicated strains. C. Mean +/- SD of capsule size, quantified as detailed in the Methods and Figure S4, with *pkr1* (37) and *ada2* (96) shown as hypercapsular and hypocapsular

controls, respectively. ****, p<0.0001 compared to KN99α by one-way ANOVA with posthoc Dunnett test.

Figure 4. Growth in mouse serum elicits increased capsule and cell wall diameter in the *pdr802* mutant. A. Light micrographs of the indicated strains after growth in mouse serum (at 37°C, 5% CO_2) for 24 h and negative staining with India ink to visualize the capsule. All images are to the same scale; scale bar, 5 µm. B. Mean +/- SD of capsule thickness, assessed by measuring at least 50 cells per strain with ImageJ. C. Cells grown as in Panel A were plated on YPD to assess CFU. Mean +/- SD of the fold-change compared to 0 h is shown. D. Mean +/- SD of cell wall diameter, measured as in B. ***, p<0.001 and ****, p<0.0001 for comparison of *pdr802* results to KN99α by one-way ANOVA with posthoc Dunnett test.

Figure 5. Absence of *PDR802* yields enlarged cells and loss of capsule induction in the context of animal infection. A. India ink staining of fungi isolated from the lungs of mice infected with the indicated strains for various times (3, 7, 14 and 18 days). All images are to the same scale; scale bar, 10 µm. B and C. Mean +/- SD of cell wall diameter (B) and capsule thickness (C), assessed by measuring at least 50 cells per strain with ImageJ. ****, p<0.0001 and ***, p<0.001 for comparison of *pdr802* results to KN99α or *PDR802* by one-way ANOVA with posthoc Dunnett test for each day post-infection.

Figure 6. Pdr802 is a negative regulator of titanisation. Left, cultures were subjected to *in vitro* conditions that induce Titan cell formation and imaged with India Ink. All images are to the same scale; scale bar, 10 µm. Images were selected so that each shows multiple examples of Titan cells, not to reflect abundance of this morphotype. Right, the percent of Titan cells (TC) in each culture was quantified using flow cytometry, gated as indicated by the blue square. FSC, forward scatter; SSC, side scatter.

Figure 7. Deletion of *PDR802* affects phagocytosis after growth under conditions that induce capsule and titan cell formation. *C. neoformans* strains were grown in YPD (18 h), DMEM (24 h), or Titan-cell induction medium (72 h) and then incubated for 2 h with J774.16 mouse macrophages; host cells were then washed and lysed to assess fungal burden by CFU. Data shown are normalized to the CFU of the initial inoculum. *, $p<0.01$ and **, $p<0.001$ compared to KN99α by one-way ANOVA with posthoc Dunnett test.

Figure 8. Interactions of Pdr802 with specific gene promoters. Read coverage for samples immunoprecipitated from tagged (light gray) and untagged (dark gray) strains. The X-axis shows the sequence position (in bp) plotted relative to the first position of the coding sequence (+1) for genes discussed in the text that encode transporters (A), transcription factors (B), and Frk102 (C). Peaks were plotted using R software (ggplot2 package).

Figure 9. Pdr802 participates in calcineurin signaling. A. ChIP-Seq results for the *HAD1* promoter, plotted as in Figure 8. B, qRT-PCR analysis of *HAD1* expression in the KN99α and *pdr802* strains after growth for 3 or 24 hours in DMEM (37°C, 5% CO_2). Results are from biological triplicates, normalized to *ACT1* expression. **, p<0.01 by one-way ANOVA with posthoc Dunnett test. C. ChIP-Seq results for the *PMC1* promoter, as in A. D. Analysis of *PMC1* expression as in B. *, p<0.05 by one-way ANOVA with posthoc Dunnett test. E. Intracellular calcium measurement by flow cytometry using Fluo-4AM. Each column shows the mean and standard deviation of three biological replicates. ***, p<0.001 and ****, p<0.0001 by one-way ANOVA with posthoc Dunnett test.

SUPPLEMENTAL FIGURE LEGENDS

Figure S1. Mutant strain construction and confirmation. A. Scheme for generating *C. neoformans* strains in the KN99α background (middle) that either lack *PDR802* (*pdr802,* top) or encode a tagged copy of the protein (*mCherry-PDR802*). B. Qualitative analysis of gene expression in Panel A strains and the complemented *pdr802* mutant (*PDR802*). Cryptococcal mRNA isolated from cells grown in DMEM (37°C, 5% CO_2, 24 hours) was used to generate cDNA; from this, segments of the genes indicated at the left were amplified using the primers listed in Data Set S2, Sheet 6, and the products were analyzed by agarose gel electrophoresis. Fragment sizes (in bp) are indicated and the ladder bands shown are 400, 500, 650, 850 and 1000 bp for the top panel; 200, 300, 400, 500, and 650 bp for the middle panel; and 100, 200, and 300 bp for the bottom panel. C. Quantitative analysis of *PDR802* expression. Samples of RNA isolated as in B were analyzed for *PDR802* expression by qRT-PCR. All results were normalized to *ACT1*

expression. Each symbol represents a biological replicate, with the mean and standard deviation also shown. ***, $p<0.001$ compared to KN99α by one-way ANOVA with posthoc Dunnett test.

Figure S2. Organ burdens. Mean +/- SD values of total colony-forming units (CFU) in the indicated tissue of mice from the Figure 1 survival curve are shown. Each point is the average value for a single animal at the time of death. For *pdr802* infections, red circles represent mice sacrificed at days 65 and 69, while blue circles represent mice sacrificed at the termination of the study (day 100). B. Mean +/- SD of total colony-forming units (CFU) in the blood and brain at the indicated times post-infection. C. Mean +/- SD of total colony-forming units (CFU) in the lung, blood and brain 75 days after infection with *pdr802*. Each color represents one mouse.

Figure S3. Characterization of *pdr802* cells. A-C.10-fold serial dilutions of WT, *pdr802*, and *PDR802* cells were plated on the media shown and incubated at 30°C (A), 37°C (B), or 37°C in the presence of 5% CO_2 (C). Nitrosative ($NaNO_2$) and oxidative (H_2O_2) stress plates were prepared with YNB medium and melanization plates containing L-DOPA were prepared as in the Methods; all other plates were prepared with YPD medium. *lac1*, a control strain lacking the ability to melanize (97). D. Urease activity of the indicated strains was evaluated using Christensen's urea solid medium (see Methods) at the indicated temperatures. *ure1*, a control strain that does not produce urease (16). E-F. Growth of the strains indicated in YPD at 30°C (E) or DMEM at 37°C and 5% CO_2 (F) was assessed by OD_{600nm} at the times indicated. G. Conditioned medium from the indicated

strains was probed for the presence of GXM after growth in DMEM for 24 or 48 hours. Immunoblotting was performed using the anti-GXM monoclonal antibody 302.

Figure S4. Semi-automated assay for cryptococcal capsule imaging. A. Schematic of applying this method to cryptococcal cells induced to form capsule by growth in DMEM (37°C, 5% CO_2) for 24 h, followed by cell wall and capsule staining. Thousands of cells may be imaged per well and analyzed automatically with software that annotates and measures the capsule (annotated in dark blue) and cell wall (annotated in bright green). See Methods for details. B. Capsule size distribution of WT cells after induction. Capsule thickness for each cell is the difference between the paired diameters of the cell wall and capsule, which is plotted with reference to the mean value. C and D. Mean and SD (C) and cumulative percentage (D) analysis of WT compared to hyper and hypocapsular control strains (here *pkr1* and *ada2*, respectively). Capsule thickness is in arbitrary units, related to the pixels measured. E. The time required to analyze the capsule thickness of 1,000 cells by this method compared to manual assessment of India ink images.

Figure S5. *PDR802* deletion induces the formation of titan cells. Mean +/- SD of (A) capsule thickness relative to cell wall diameter and (B) capsule diameter, assessed by measuring at least 50 cells per strain with ImageJ. ***, $p<0.001$ and ****, $p<0.0001$ for comparison of *pdr802* results to KN99α or *PDR802* by one-way ANOVA with posthoc Dunnett test for each day post-infection. C. Percent of Titan cells in the indicated strain, evaluated using various published parameters: cell wall diameter bigger than 10 or 15 µm (19) or capsule diameter bigger than 30 µm (41).

Figure S6. Viability of tagged-Pdr802 strains in DMEM. The indicated strains were grown in DMEM at 37°C and 5% CO_2 for the times shown and samples were tested for their ability to form colonies on YPD medium. Plotted is the fold-change in CFU relative to the initial culture.

Figure S7. Pdr802 DNA-binding motif and target validation. A. Pdr802-binding motifs determined using DREME (72). Primary and secondary hits are shown for analysis of 1,000 bp upstream of the initiating ATG (top two rows) or that region plus the next 200 bp (lower two rows). RC, reverse complement. B. Expression of the indicated genes in KN99α (filled bars) and *pdr802* (open bars) cells, grown in host-like conditions for the times shown. qRT-PCR results are normalized to *ACT1* expression; mean and standard deviation of three biological replicates for each time point are shown. **, $p<0.01$ compared to KN99α by one-way ANOVA with posthoc Dunnett test. *CNAG_03304* encodes a hypothetical protein and *CNAG_07402* a pantothenate transporter.

Data Set S1. Pdr802 ChIP-Seq data. Data in sheets 1-3 is limited to genes that showed >2-fold enrichment when Chip-Seq was performed on strains expressing tagged versus untagged Pdr802. Sheet 1, annotated peaks that occur in gene promoter regions. Sheet 2, ChIP-Seq data for Sheet 1. Sheet 3, all peaks, annotated (not restricted to promoter regions). Sheet 4, ChIP-Seq data of Pdr802-specific peaks. Sheet 5, ChIP-Seq data of all peaks in mCherry-Pdr802 samples. Sheet 6, ChIP-Seq data of all peaks in untagged

(WT) control samples. Sheet 7, GO analysis of genes enriched >2-fold in ChIP-Seq studies. Sheet 8, transmembrane transporters identified as Pdr802 targets by ChIP-Seq.

Data Set S2. Pdr802 binding motifs, target analysis, and primers used in this study. Sheet 1, Pdr802 binding motifs in genes that are down-regulated during Titan cell formation *in vitro*. Sheet 2, gene ontology analysis for genes that are differentially expressed during Titan cell formation *in vitro*. Sheet 3, Pdr802 binding motifs in genes that are up-regulated during Titan cell formation *in vitro*. Sheet 4, Pdr802 binding motifs in the promoters of *HAD1* and *PMC1*. Sheet 5, the intersection of Pdr802 targets and genes that are Crz1-independent calcineurin targets under conditions thermal stress (55). Sheet 6, primers used in this study. Fold enrichment and adjusted p (q) values throughout are for the ChIP-Seq results.

Supplementary Methods.

FIGURE 1

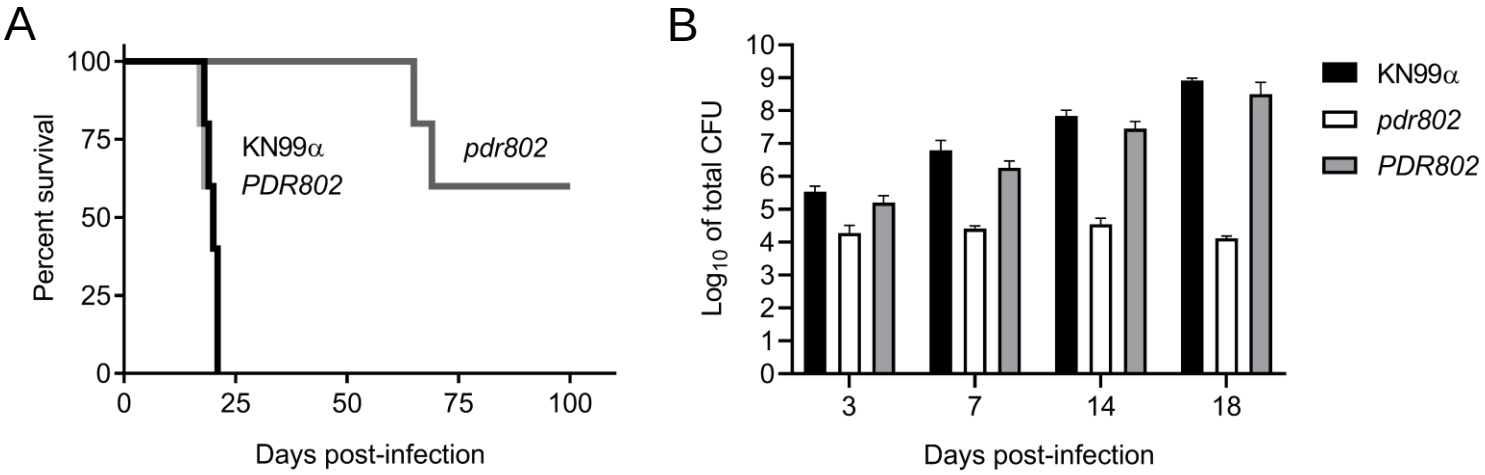
A
Percent survival
100
75
50
25
0
0
25
50
75
100
Days post-infection
KN99α
PDR802
pdr802
B
Log10 of total CFU
10
9
8
7
6
5
4
3
2
1
0
3
7
14
18
Days post-infection
KN99α
pdr802
PDR802

FIGURE 2

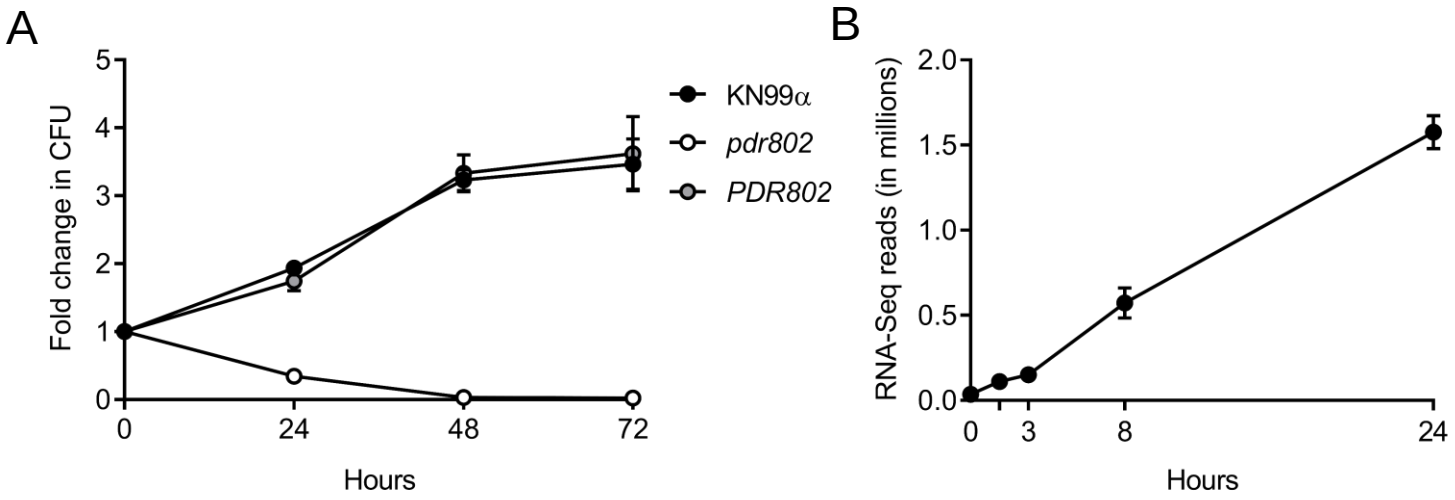
A
Fold change in CFU
5
4
3
2
1
0
0
24
48
72
Hours
KN99α
pdr802
PDR802
B
RNA-Seq reads (in millions)
2.0
1.5
1.0
0.5
0.0
0
3
8
24
Hours

FIGURE 3

A

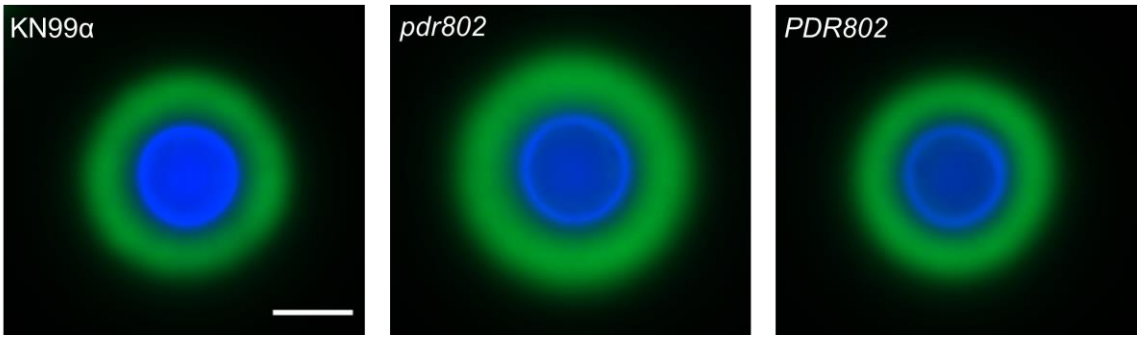
KN99α
pdr802
PDR802

B

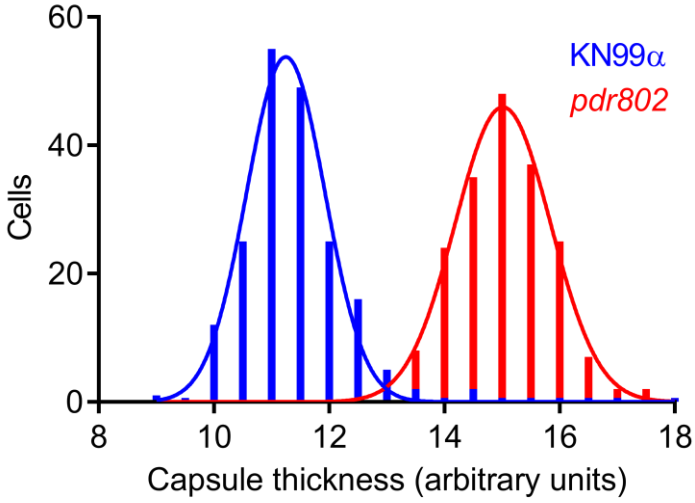
60
40
20
0
Cells
8
10
12
14
16
18
Capsule thickness (arbitrary units)
KN99α
pdr802

C

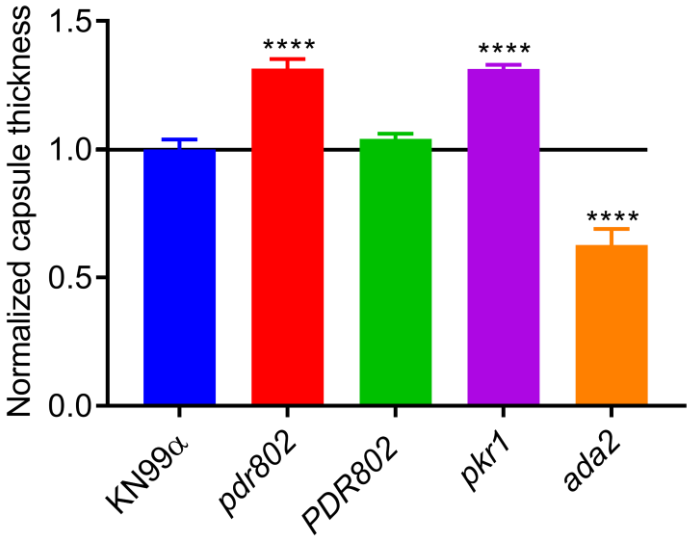
1.5
1.0
0.5
0.0
Normalized capsule thickness
****
****
****
KN99α
pdr802
PDR802
pkr1
ada2

FIGURE 4

A

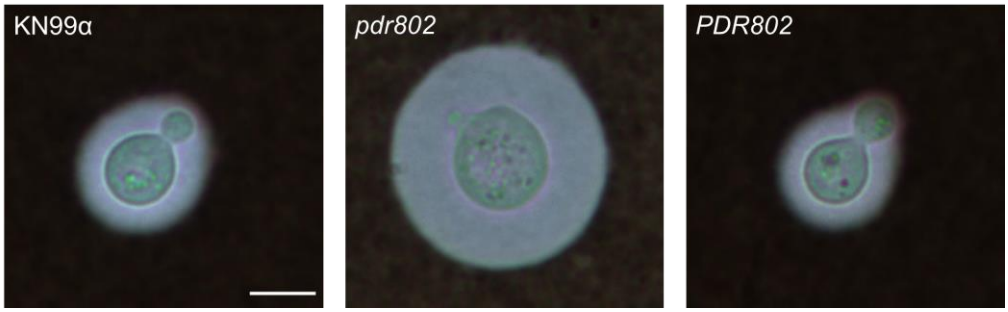

B

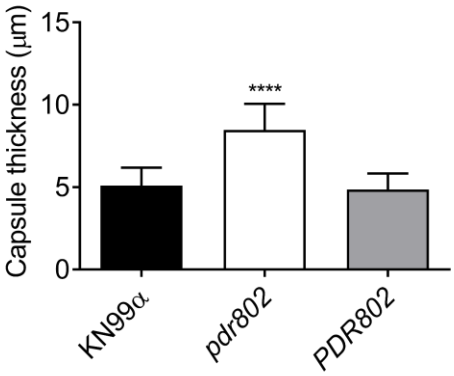

C

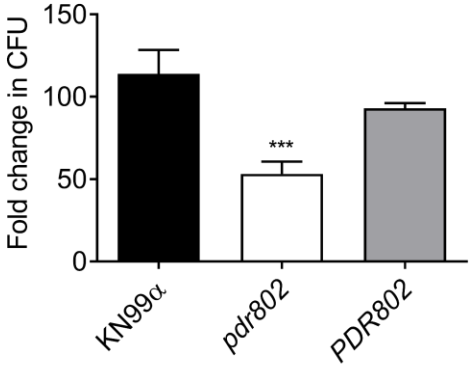

D

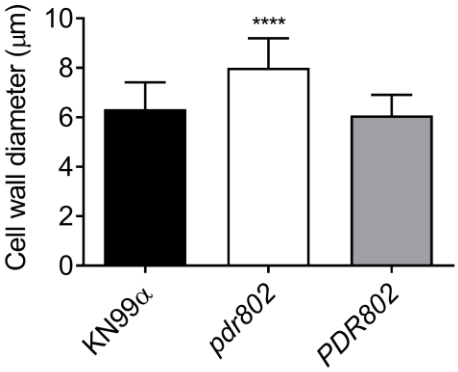

FIGURE 5

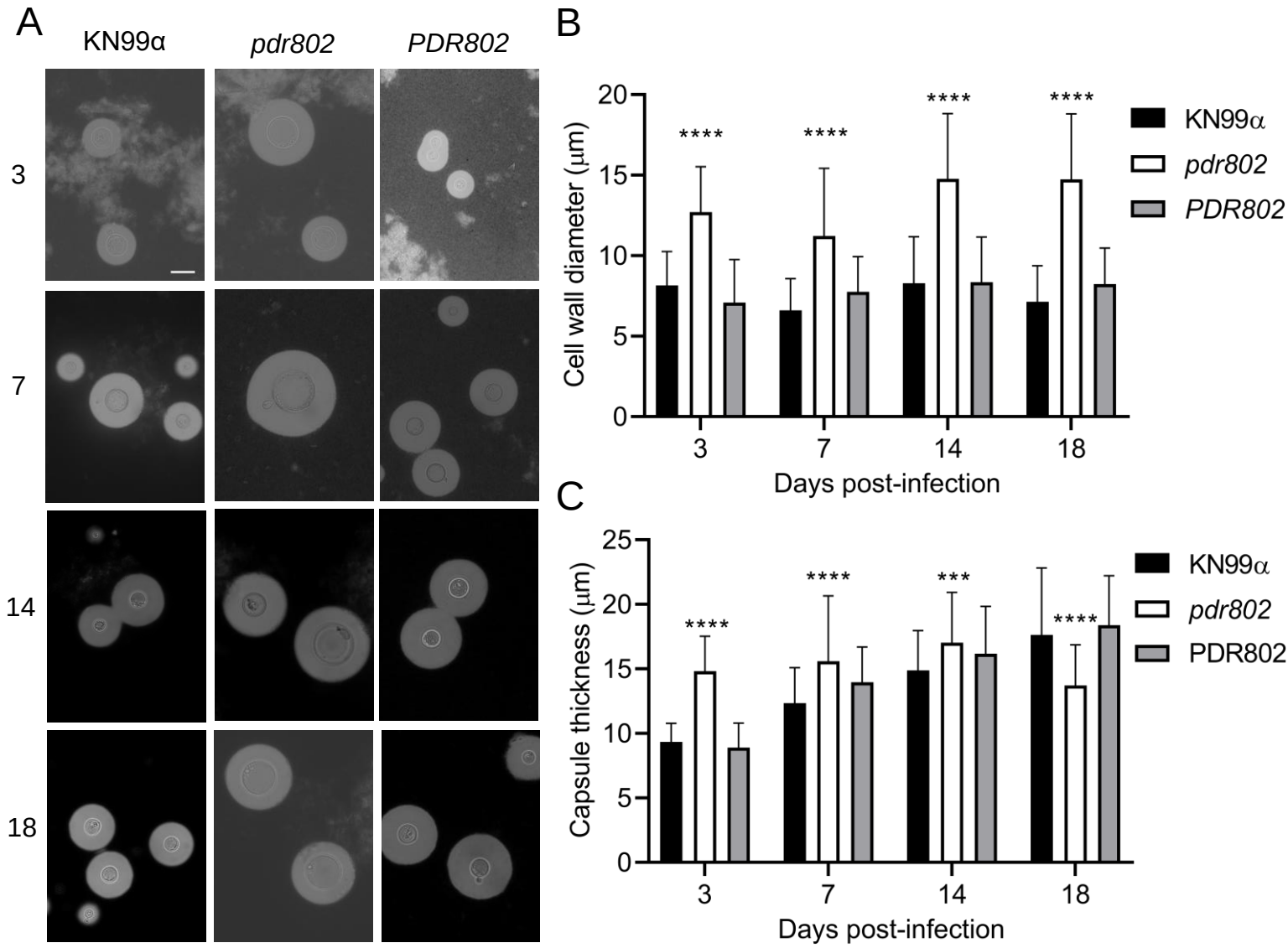
A
KN99α
pdr802
PDR802
3
7
14
18
B
Cell wall diameter (μm)
20
15
10
5
0
****
****
****
****
3
7
14
18
Days post-infection
KN99α
pdr802
PDR802
C
Capsule thickness (μm)
25
20
15
10
5
0
****
****
***
****
3
7
14
18
Days post-infection
KN99α
pdr802
PDR802

FIGURE 6

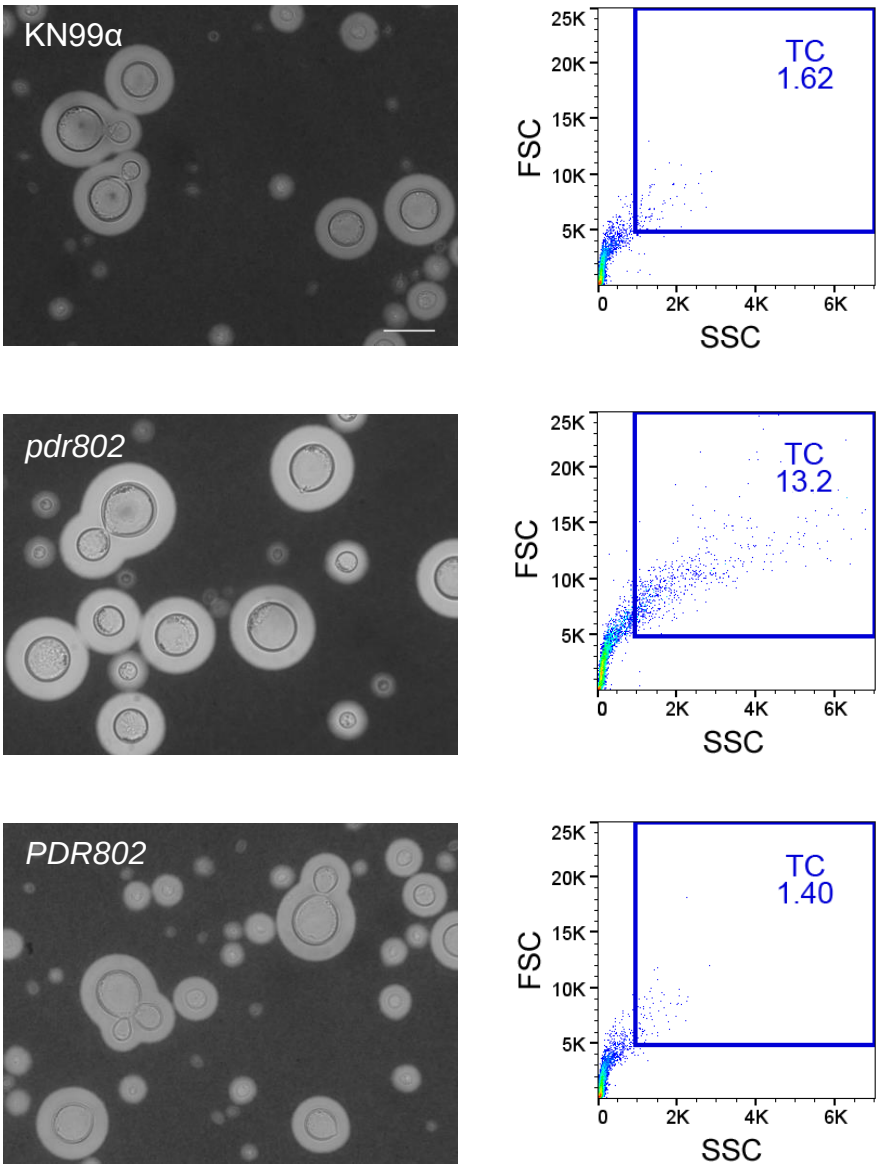
KN99α
TC
1.62
FSC
SSC
25K
20K
15K
10K
5K
0
2K
4K
6K
pdr802
TC
13.2
FSC
SSC
PDR802
TC
1.40
FSC
SSC

FIGURE 7

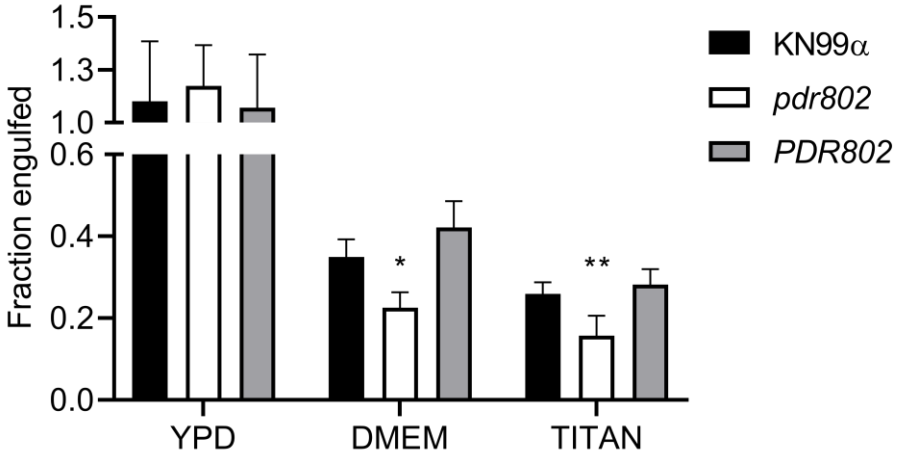
1.5
1.3
1.0
0.6
0.4
0.2
0.0
Fraction engulfed
*
**
YPD
DMEM
TITAN
KN99α
pdr802
PDR802

FIGURE 8

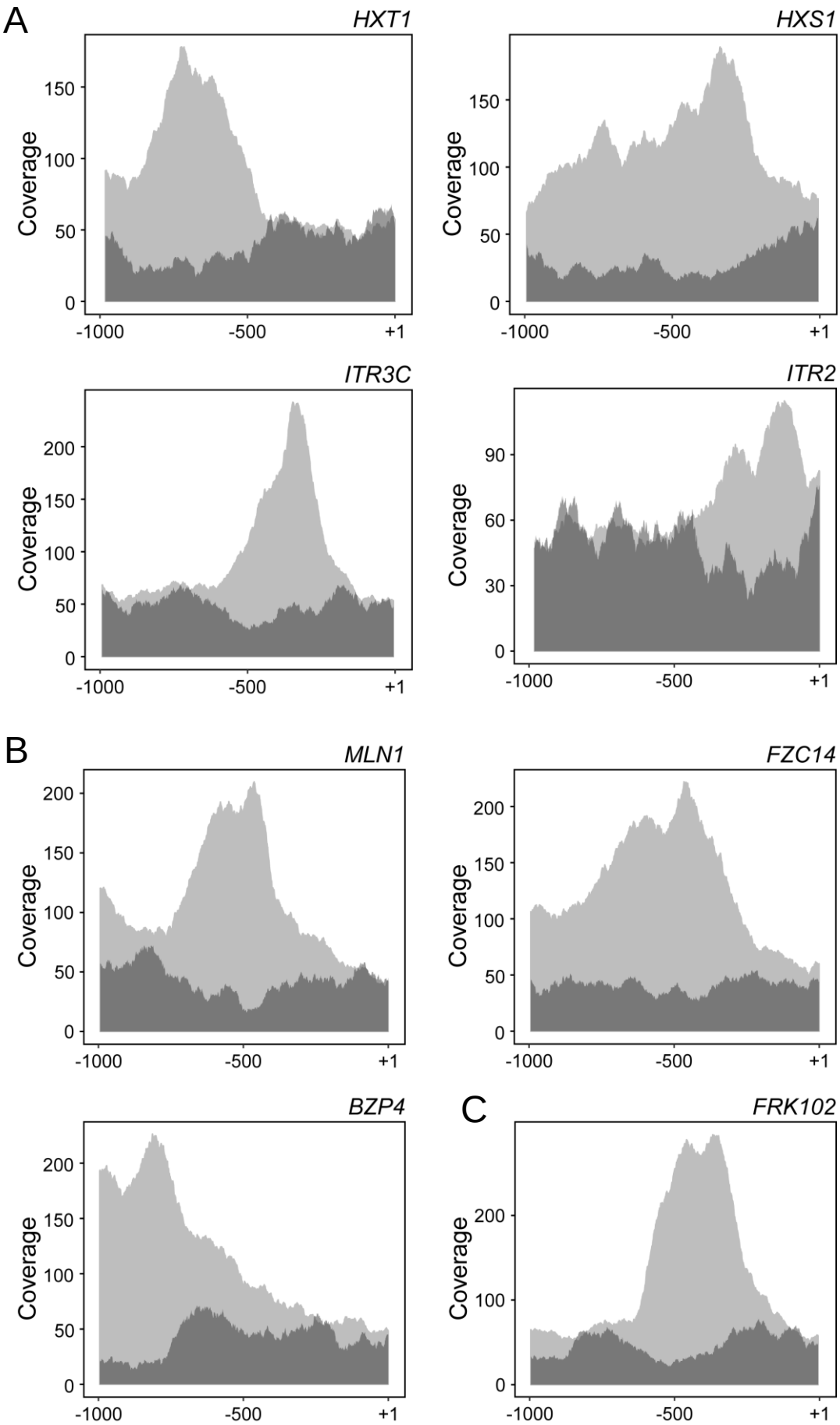
A
HXT1
HXS1
ITR3C
ITR2
B
MLN1
FZC14
BZP4
C
FRK102
Coverage
-1000
-500
+1

FIGURE 9

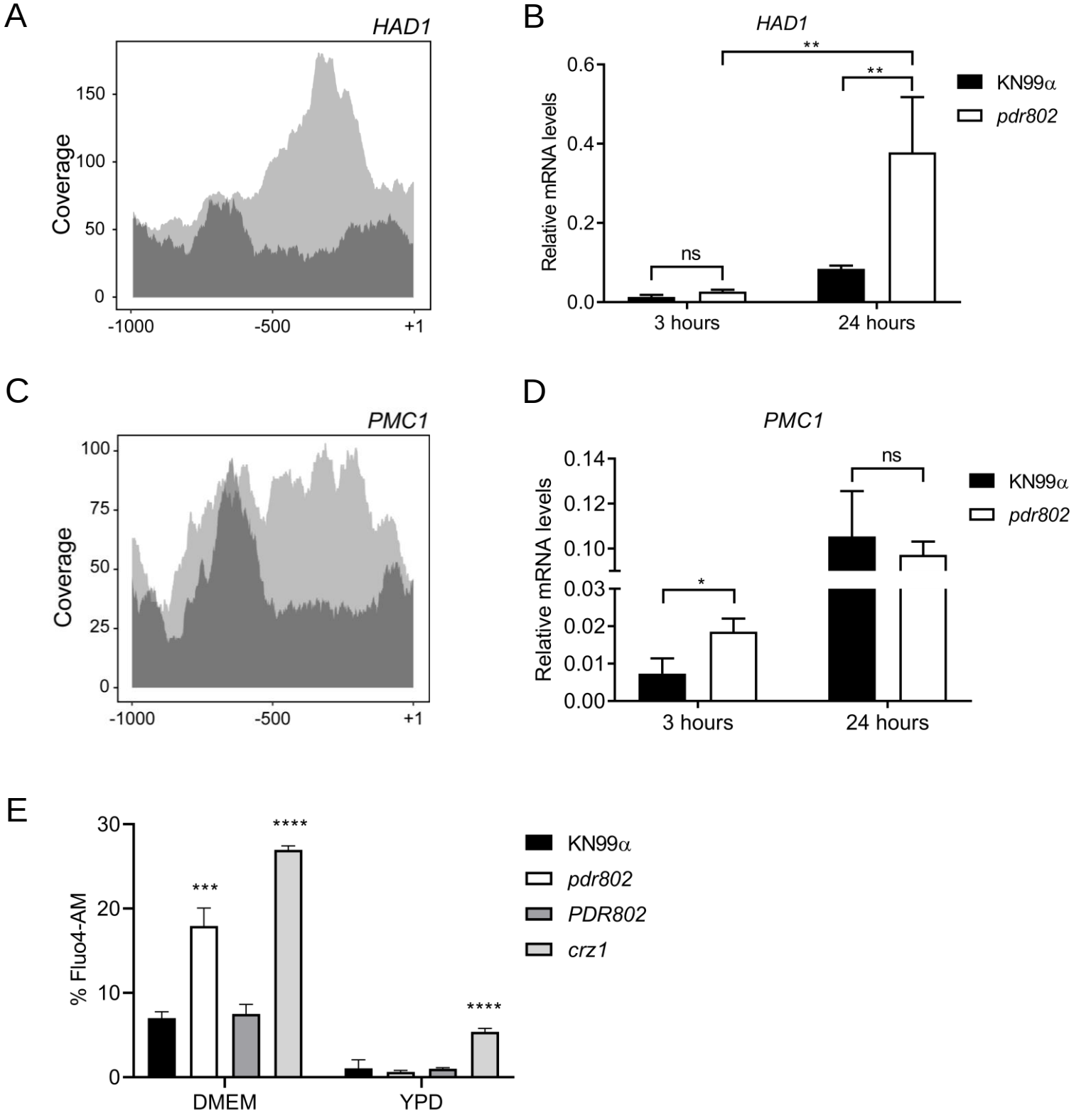
A
HAD1
Coverage
150
100
50
0
-1000
-500
+1
B
HAD1
Relative mRNA levels
0.6
0.4
0.2
0.0
**
**
ns
3 hours
24 hours
KN99α
pdr802
C
PMC1
Coverage
100
75
50
25
0
-1000
-500
+1
D
PMC1
Relative mRNA levels
0.14
0.12
0.10
0.03
0.02
0.01
0.00
ns
*
3 hours
24 hours
KN99α
pdr802
E
% Fluo4-AM
30
20
10
0
***
****
****
DMEM
YPD
KN99α
pdr802
PDR802
crz1